



Faculty of Science and Technology
MESA⁺ Research institute
Group Inorganic Materials Science
M. Sc. Thesis



**Designing an oxygen coulometric
titration set-up to study mixed-
conducting perovskites**



George van der Donk
University of Twente
P.O. Box 217
7500 AE Enschede
The Netherlands
Internet: www.ims.tnw.utwente.nl
Period September 2003 – May 2004

Designing an oxygen coulometric titration set-up to study mixed-conducting perovskites

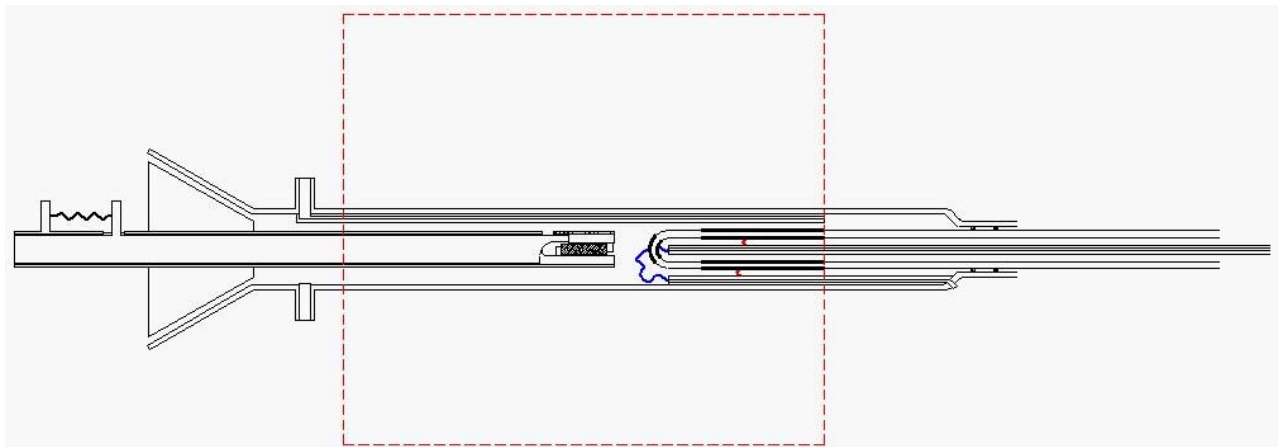
M. Sc. Thesis

By

George van der Donk

Enschede

11 May 2004



Schematic overview of the coulometric titration set-up designed by:
George van der Donk

Graduation Committee:

Prof. Dr. Ing. D.H.A. Blank (chairman)

Ing. F.H.B. Mertins (supervisor)

Dr. B.A. Boukamp

Dr. N. Bonanos (Risø National Laboratory, Denmark)

Dr. H.J.M. Bouwmeester

Summary

The objective of this D-subject was to construct a set-up for coulometric titration experiments, and to measure the electronic conductivity of selected mixed-conducting perovskites as a function of the oxygen partial pressure. A standard 4-point 'Van der Pauw' technique was employed to measure the electrical conductivity.

The electrical conductivity of mixed-conducting perovskites was studied successfully in a large oxygen partial pressure range at different temperatures with the use of coulometric titration. The coulometric titration set-up was designed with easy exchange of samples. The set-up temperature range is 975 to 1175 K and the lowest obtained oxygen partial pressure is $1 \cdot 10^{-16}$ atm.

The oxygen leakage is about 0.4 μA at 1075 K at an oxygen partial pressure of $1 \cdot 10^{-5}$ atm and is in agreement with the literature data of 0.5 μA . The oxygen leakage is controlled by the mechanical leakage through the 'Torr seal'. However, the oxygen partial pressure is not completely under control due to processes that decrease the oxygen partial pressure with time.

The conductivity of $\text{La}_{0.95}\text{Sr}_{0.05}\text{CoO}_{3-\delta}$ is $1.0 \cdot 10^3$ S/cm at an oxygen partial pressure of $1 \cdot 10^{-5}$ atm at 1065 K and is in agreement with literature. The conductivity of $\text{La}_{0.95}\text{Sr}_{0.05}\text{CoO}_{3-\delta}$ decreases with the oxygen partial pressure due to the increase of oxygen vacancies and the reduction of the cobalt. The conductivity of $\text{La}_{0.95}\text{Sr}_{0.05}\text{CoO}_{3-\delta}$ is independent in an oxygen partial pressure range of $1 \cdot 10^{-6}$ to $1 \cdot 10^{-12}$ atm at 1065 K. $\text{La}_{0.95}\text{Sr}_{0.05}\text{CoO}_{3-\delta}$ decomposes below an oxygen partial pressure of to $1 \cdot 10^{-12}$ atm at 1065 K.

The conductivity of $(\text{La}_{0.8}\text{Ca}_{0.2})_{1.01}\text{FeO}_{3-\delta}$ decreases with decreasing oxygen partial pressure and increasing temperature in the near atmospheric condition. The conductivity of $(\text{La}_{0.8}\text{Ca}_{0.2})_{1.01}\text{FeO}_{3-\delta}$ is 38 S/cm at an oxygen partial pressure of $1 \cdot 10^{-5}$ atm at 1175 K and is higher than the conductivity of $\text{La}_{0.9}\text{Sr}_{0.1}\text{FeO}_{3-\delta}$ (2 S/cm) in similar conditions. The activation energy of the electrical conductivity of $(\text{La}_{0.8}\text{Ca}_{0.2})_{1.01}\text{FeO}_{3-\delta}$ is 50 KJ/mol and is in agreement with the literature.

Table of contents

1. INTRODUCTION	3
1.1. History	3
1.2. Assignment	4
2. PRINCIPLE OF OXYGEN COULOMETRIC TITRATION	5
2.1. Electrochemical cell	5
2.1.1. Oxygen leakage	6
2.1.2. Non-Nernstian behaviour of a solid electrolyte	7
2.2. Diffusion and kinetics	8
2.2.1. Oxygen ion diffusion in the sample	8
2.2.2. Surface reaction	9
2.2.3. Oxygen gas diffusion	9
2.3. Non-stoichiometry and conductivity measurements	10
3. EXISTING COULOMETRIC TITRATION SET-UPS	12
3.1. Oxygen pump and sensor design	12
3.2. Similarities and differences in coulometric titration set-ups	13
3.3. Problems and challenges in coulometric titration	14
4. DEFECT CHEMISTRY OF MIXED CONDUCTING PEROVSKITES	16
4.1. Lanthanum based perovskites	16
4.1.1. Non-stoichiometry of $\text{La}_{1-x}\text{Sr}_x\text{FeO}_{3-\delta}$	17
4.1.2. Conductivity in $\text{La}_{1-x}\text{Sr}_x\text{FeO}_{3-\delta}$	19
4.2. $\text{La}_{0.95}\text{Sr}_{0.05}\text{CoO}_{3-\delta}$	20
4.3. $(\text{La}_{0.8}\text{Ca}_{0.2})_{1.01}\text{FeO}_{3-\delta}$	21
5. EXPERIMENTAL	22
5.1. Sample preparation	22
5.2. Design of the coulometric titration set-up	22
5.2.1. Cell	22
5.2.2. Oxygen sensor and pump	23
5.2.3. Sample holder	24
5.2.4. Sealing	25
5.2.5. Gas system	25
5.2.6. Electrical equipment	25
5.3. Development of the coulometric titration set-up	26
5.3.1. Cell / sealing	27
5.3.2. Oxygen sensor and pump	27
5.3.3. Sample holder	27
6. RESULTS	29
6.1. XRD $(\text{La}_{0.8}\text{Ca}_{0.2})_{1.01}\text{FeO}_{3-\delta}$	29
6.2. Oxygen leakage	29
6.3. Oxygen absorption	33
6.4. Conductivity	34
6.4.1. $\text{La}_{0.95}\text{Sr}_{0.05}\text{CoO}_{3-\delta}$	34
6.4.2. $(\text{La}_{0.8}\text{Ca}_{0.2})_{1.01}\text{FeO}_{3-\delta}$	35

7. DISCUSSION	37
7.1. Design	37
7.2. Conductivity	38
7.2.1. $\text{La}_{0.95}\text{Sr}_{0.05}\text{CoO}_{3-\delta}$	39
7.2.2. $(\text{La}_{0.8}\text{Ca}_{0.2})_{1.01}\text{FeO}_{3-\delta}$	39
8. CONCLUSION	40
8.1. Design	40
8.2. Conductivity	40
9. RECOMMENDATIONS	41
10. SYMBOLS	43
11. REFERENCE	45
12. DANKWOORD	49
APPENDIX A – COULOMETRIC TITRATION SET-UPS	50
Sockel et al.	50
Piekarczyk et al.	50
Porat, Riess and co-workers	51
Gür and Belzner and co-workers	53
Lankhorst	53
Lade and Jacobsen	54
Mizusaki et al.	55
Tikhonovich et al.	55
Tanesescu et al.	56
Li et al.	57
Bakken	58
Ferreira et al.	58
Figueiredo et al.	58
Zhang et al.	59
Ohly et al.	59
Mitberg, Poeppelmeier and co-workers.	61
Ochin et al.	61
APPENDIX B – EDX RESULTS OF THE PLATINUM-PASTE	63
APPENDIX C – MICRO COULOMETRIC TITRATION CELL	64
APPENDIX D - DEFECT CHEMISTRY OF YSZ	66

1. Introduction

Mixed-conducting perovskite oxides have potential applications as gas sensors, oxygen permeable dense membranes and solid oxide fuel cells. The partial ionic and electronic conductivities are controlled via the defect chemistry exhibited by the materials. Oxygen coulometric titration (CT) allows precise control of the oxygen activity in the surrounding gas phase of the material and, hence, enables direct control of the oxygen non-stoichiometry as function of oxygen partial pressure.

1.1. History

The advantage of coulometric titration is the use of a universal reagent, the electron [1]. The electron behaviour can be controlled and measured easily and accurately. The electron can form a direct electrochemical reaction on the electrode or it can react with other reactants. Faraday reported the basis of coulometric titration by stating in 1833: “The chemical power of a current of electricity is in direct proportion to the absolute quantity of electricity which passes.” Due to the work of Faraday and his researches, we now use the terms ions, cation, anion, electrode and electrolyte. The term ‘coulometric analyses’ was used introduced by Szebelledy et al. [2] in 1938, they used this term to design a quantitative determination of the quantity of electricity required to complete a reaction in an electrolysis cell.

At first, several research groups (e.g. Tackett [1]) applied coulometric titration on solutions. Wagner [3] was the first who reported in 1953 that coulometric titration could also be used on solids. The electrolyte transports electrons and the counter current is an anion, commonly oxygen anions sulphide. Wagner used the Nernst equation to determine the potential difference required to obtain a difference in oxygen fugacity:

$$EMF = \frac{RT_{electrolyte}}{4F} \ln \left(\frac{f_{O_2}^{ref}}{f_{O_2}^{Cell}} \right) \quad (1)$$

Thermogravimetry is used commonly to study the oxygen non-stoichiometry as a function of temperature and oxygen partial pressure. However, the oxygen non-stoichiometry can be determined more accurately with the use of coulometric titration. Coulometric titration enables to study the exact amount of oxygen added or remove from the sample. The amount of oxygen is an equivalent of the monitored electrical currents and potentials.

Besides that, coulometric titration permits direct control of the oxygen partial pressure environment in which the sample is placed. Another advantage is that the chemical diffusion coefficients can be determined by measuring the rate at which the electrochemical cell proceeds to equilibrium [4]. Therefore, coulometric titration is a useful tool to study the thermodynamics and the defect chemistry of materials.

The principle of coulometric titration is discussed in chapter 2; and contains the electrochemistry, diffusion and different kinds of measurements with on samples. Most of the coulometric titration set-ups found in literature are summarized in chapter 3 CT-designs. The defect chemistry is discussed in chapter 4. The manufacturing and testing of the coulometric titration set-up is reported in chapter 5 experimental. The oxygen leakage rate and conductivity measurements of $La_{0.95}Sr_{0.05}CoO_{3-\delta}$ and $(La_{0.8}Ca_{0.2})_{1.01}FeO_{3-\delta}$ is overviewed in chapter 6 results and the result, design and developments of the coulometric titration set-up is discussed in chapter 7.

1.2. Assignment

‘Oxygen coulometric titration of mixed conducting perovskites’

The objective of this D-subject is to construct a set-up for coulometric titration experiments, and to measure the electronic conductivity of selected mixed-conducting perovskites as a function of the oxygen partial pressure. A standard 4-point ‘Van der Pauw’ technique will be employed to measure the electrical conductivity.

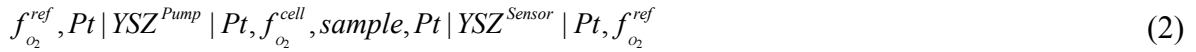
Project:

- Write a literature report, which should cover
 - a. principle of oxygen coulometric titration (keywords: technique, materials, information to be retrieved (defect chemistry))
 - b. experimental problems (oxygen semi-permeability of electrolyte, accessible range of oxygen partial pressure, buffering gases)
 - c. Electrical conductivity measurements (2-probe versus 4-probe measurements, Van der Pauw technique)
- Design and construction of an experimental set-up
- Testing and evaluation of the experimental set-up
- Preparation of selected perovskite samples
- Measurement and interpretation of the pO_2 -dependent conductivity

2. Principle of oxygen coulometric titration

2.1. Electrochemical cell

Coulometric titration measures and controls the oxygen fugacity in a sealed environment [5]. A sample is placed in a sealed electrochemical cell constructed with an electrolyte (e.g. YSZ) and two electrodes (e.g. Pt). The electrolyte allows fast oxygen ion transport and therefore transports oxygen anions between the (sealed) cell volume and its environment. An experimental arrangement of a double electrochemical cell for a coulometric titration set-up can be represented as [4]:



The Gibbs energy of the cell can be given as:

$$\Delta G_{Cell} = \mu_{O_2}^{cell} - \mu_{O_2}^{ref} = 4F \cdot EMF \quad (3)$$

The oxygen chemical potential (in the cell or as reference gas) is:

$$\mu_{O_2} = \mu_{O_2}^0 + RT \ln f_{O_2} \quad (4)$$

Substituting equation (4) in equation (3) will generate the Nernst-equation (5). The ratio between the oxygen fugacity in the cell and the oxygen fugacity of the reference determines the electromotive force (EMF or cell voltage E) across the electrolyte:

$$EMF = \frac{RT}{4F} \ln \left(\frac{f_{O_2}^{ref}}{f_{O_2}^{Cell}} \right) \quad (5)$$

The oxygen fugacity can be considered equal to the oxygen partial pressure in the cell and of the reference in the case of a standard state of 1 atm total pressure, similar temperature on both electrodes [6].

The oxygen fugacity of the reference gas is known (e.g. pure oxygen or air), the oxygen fugacity inside the cell can thus be determined from the obtained EMF. This is the principle of an oxygen sensor. The oxygen concentration in the cell volume can be controlled by electrochemically pumping oxygen in or out of the cell through the electrolyte by applying (instead of measuring) a potential. Equation (6) describes the electrochemical reaction at the electrode and presents the principle of the oxygen pump, see Figure 1.



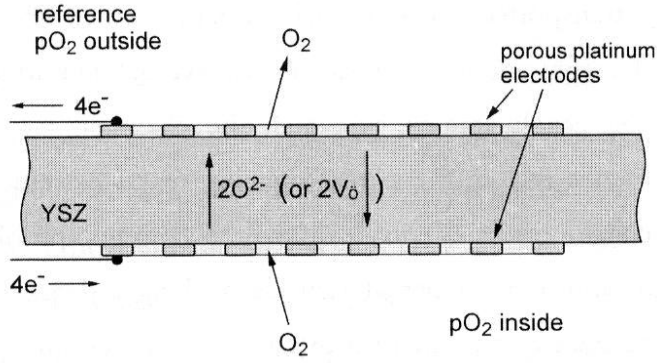


Figure 1: A schematic drawing of an electrochemical oxygen pump [7].

The Nernst-equation (5) can be used if the following requirements are fulfilled:

1. The charge transfer across the electrolyte occurs strictly in an oxygen anions (O^{2-}) transport, indirectly by oxygen vacancies (V_o^{**}).
2. The equipment connected to the electrodes have a relative large resistance compared to the electrochemical cell, thus no current is obtained.
3. There are no undesired chemical reactions that changes the composition of the gases significantly on the electrolyte and electrodes [8].

The transported electrical current (I) determines the oxygen concentration step (change) in the cell (oxygen in the gas phase and oxygen in the sample):

$$\Delta n_{O_2}^{Cell} = \Delta n_{O_2}^{Sample} + \Delta n_{O_2}^{Gas} = -\frac{1}{2F} \int_{t_1}^{t_2} I dt \quad (7)$$

Equation (7) can also be written in terms of oxygen molecules:

$$\Delta n_{O_2}^{Cell} = -\frac{1}{4F} \int_{t_1}^{t_2} I dt \quad (8)$$

Every electrolyte experience a semi-permeation oxygen leakage, which can be included in equation (7):

$$\Delta n_{O_2}^{Cell} = n_{O_2}^{Leakage} - \frac{1}{2F} \int_{t_1}^{t_2} I dt = \frac{1}{2F} \int_{t_1}^{t_2} (I_{Leakage} - I) dt \quad (9)$$

The factor ' $n_{O_2}^{Leakage}$ ' is the number of oxygen moles that has leaked through the electrolyte due to semi permeability of the electrolyte.

2.1.1. Oxygen leakage

Oxygen leakage is unavoidable in a coulometric titration set-up because of the difference in oxygen partial pressure inside and outside the cell at high temperature. The oxygen can leak into the cell through sealants (hereafter referred as mechanical oxygen leakage) and through the electrolyte. The electrolyte is mainly an ion conductor, however the electrolyte

experiences a small electronic conduction at high temperature and therefore shortcutting occurs. This shortcutting results in oxygen leakage, however, in case of an YSZ electrolyte, it only occurs significantly above 1000 K or with large gradient in oxygen partial pressures across the electrolyte.

The oxygen leakage should be known at every temperature and oxygen partial pressure difference to determine corrections required to perform accurate coulometric titration measurements. The oxygen leakage can be counterbalanced by a constant oxygen pumping to maintain a steady oxygen partial pressure environment [5]. Oxygen leakage is presented by a leakage current. This leakage current is equal the current required to maintain a stable oxygen partial pressure in the cell. The theoretical relation for electrochemical leakage through YSZ electrolyte is given by Bouwmeester et al. [9], equation (10). The ‘ α ’ is a function of temperature and electrolyte properties.

$$I_{Leakage} = \alpha \left[\left(p_{O_2}^{ref} \right)^{\frac{1}{4}} - \left(p_{O_2}^{cell} \right)^{\frac{1}{4}} \right] \quad (10)$$

2.1.2. Non-Nernstian behaviour of a solid electrolyte

Non-Nernstian behaviour occurs e.g. when the electrolyte is not a pure ionic conductor. The electrical conductivity compared to the ionic conductivity is related to the (electrical) transference number, see equation (11) and (12).

$$t_i = \frac{\sigma_i}{\sigma_e + \sigma_i} \quad (11)$$

$$\sigma_{tot} = \sigma_i + \sigma_e = t_e \sigma_{tot} + t_i \sigma_{tot} \quad (12)$$

The transference number of electrons is similar to equation (11); the nominator is then replaced by the electric conductivity.

A solid electrolyte loses its pure ionic conductivity at a certain temperature and oxygen partial pressure, where it becomes a mixed conductor. The most commonly used electrolyte is zirconia stabilised with ~8 mol % yttria. Yttrium acts as an acceptor. The defect chemistry of yttrium stabilized zirconia is described in appendix D.

The lower oxygen partial pressure limit where calcium stabilized zirconia becomes a mixed conductor is at a temperature of 1173 K and oxygen partial pressure is $1 \cdot 10^{-24}$ atm. The electron transference number ' t_e ' is larger than 0.01 if the temperature is higher at the mentioned oxygen partial pressure or the oxygen partial pressure is lower at that temperature [10, 11]. Iwase et al. [10] studied the P_Θ (the oxygen partial pressure where the ionic and electrical conductivity are equal) of yttria (6 and 8 mol %) doped zirconia with the use of a CT cell, see Figure 2. The P_Θ value for 8 mol% yttria doped zirconia is 10^{-14} atm at 1873 K and 10^{-32} atm at 1273 K [10]. However, the electronic conductivity is highly dependent on the impurities in the material. These impurities can block the stabilising property of yttrium in zirconia or form a second phase.

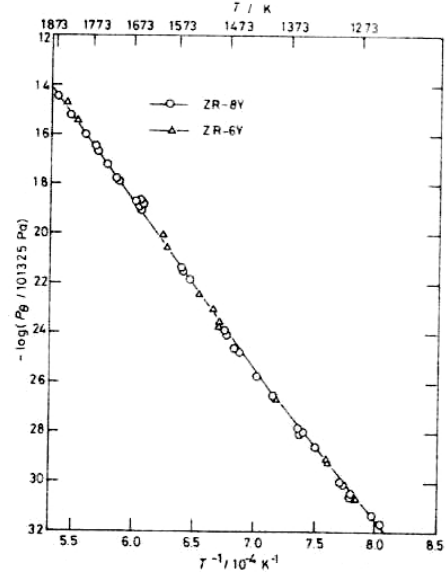


Figure 2: P_Θ of yttria (6 and 8 mol %) stabilised zirconia at the oxygen partial pressure versus reciprocal temperature [10]

2.2. Diffusion and kinetics

The oxygen diffusion in the sample or in the gas phase and the oxygen surface exchange coefficients can be determined with the use of a coulometric titration set-up. The equilibration time after an oxygen partial pressure step is monitored. The oxygen diffusion in the gas phase, the surface reaction and the diffusion in the gas phase can determine this equilibration time. This equilibration time is highly dependent on the temperature [7].

2.2.1. Oxygen ion diffusion in the sample

Oxygen ions diffuse in the bulk of a mixed-conducting oxide if there is an oxygen chemical potential gradient [12]. The equilibration time for this diffusion process can be determined with coulometric titration. The oxygen flux J_O is related to the gradient in oxygen chemical potential ' μ_{O_2} ' as given by the Wagner [13] equation:

$$J_O = -\frac{1}{8F^2} \sigma_o t_e \nabla \mu_{O_2} \quad (13)$$

To describe the non-steady state transport of oxygen, the equation (13) is often rewritten in terms of oxygen concentration gradient ∇c_O :

$$J_O = -\tilde{D} \nabla c_O \quad (14)$$

Where ' \tilde{D} ' is the chemical diffusion coefficient for oxygen in predominantly electronic conducting samples ($t_e \approx 1$) and can be given as:

$$\tilde{D} = \frac{\sigma_o}{8F^2} \left(\frac{\partial \mu_{O_2}}{\partial c_O} \right) \quad (15)$$

The term between brackets can be obtained independently by measuring the oxygen non-stoichiometry of the sample as a function of its oxygen chemical potential at equilibrium by substituting equation (15) in the Nernst-Einstein equation. The conductivity of oxygen ions is: (The oxygen valence (z_O) is -2 .)

$$\sigma_o = \frac{D_o c_o z_o^2 F^2}{RT} \quad (16)$$

The relation between the component diffusion coefficient D_O and the chemical diffusion coefficient \tilde{D} can be given as:

$$\tilde{D} = D_o \left(\frac{1}{2} \frac{\partial \ln P_{O_2}}{\partial \ln c_o} \right) \quad (17)$$

The oxygen ion transport is assumed to occur via a hopping process over vacant oxygen sites [12]. If all the vacancies are equivalent then the chemical diffusion coefficient can be written as function of the ‘ \tilde{D} ’ vacancies diffusion coefficient:

$$\tilde{D} = D_v \left(-\frac{1}{2} \frac{\partial \ln P_{O_2}}{\partial \ln c_v} \right) \quad (18)$$

2.2.2. Surface reaction

The exchange of oxygen between the oxide surfaces and the gas phase can involve series of reaction steps of which any can be rate determining [13]. The reaction steps include adsorption, dissociation, charge transfer, surface diffusion of intermediate species of oxygen and, incorporation in the surface layer. Generally, the surface reaction of oxygen is associated with transport of charge.

A possible scheme for the surface kinetics of a mixed-conductor is presented in equations (19) to (23):



The mechanism and the rate of surface kinetics may vary from material to material and can be determined with coulometric titration. The equilibriums in equation can be written with equilibrium constants and these have specific activation energies.

2.2.3. Oxygen gas diffusion

Oxygen diffusion in the gas phase is likely to be fast compared to the oxygen diffusion in the bulk of the sample. The oxygen diffusion in the gas phase in case of different concentrations and can be described with the first Fick's Law:

$$j = -\tilde{D} \frac{\partial c}{\partial x} \quad (24)$$

The oxygen diffusion in the gas phase is dependent on the diffusion coefficient, which is a function of temperature, the concentration difference (c) and, the distance (x). In case of a tube, the distance is mostly dependent on the length of the tube and the amount of dead volume.

2.3. Non-stoichiometry and conductivity measurements

The non-stoichiometry is determined by the amount of oxygen in the metal. The oxygen added or removed to the cell is precisely known. The oxygen sensor measures the oxygen partial pressure. This oxygen concentration can be calculated with the oxygen partial pressure in the gas phase and the effective volume see equation (25). The difference between the added oxygen moles and the increase of oxygen moles in the gas phase must be adjusted to the sample. The temperature in the cell is not constant. Therefore the total oxygen content can not be derived from the ideal gas law. The oxygen partial pressure step, the obtained oxygen pump current and the oxygen leakage must be known to determine the effective volume.

$$\Delta n_{O_2}^{Cell} = n_{O_2}^{Leakage} - \frac{1}{2F} \int_{t_1}^{t_2} I dt - \frac{1}{R} \left(\frac{V}{T} \right)_{eff} (P_{O_2}^f - P_{O_2}^i) \quad (25)$$

The non-stoichiometry ‘ $\Delta\delta$ ’ of the sample can be written as:

$$\Delta\delta = \frac{m_{molar\ mass}}{m_{sample}} \cdot \left(n_{O_2}^{Leakage} - \frac{1}{2F} \int_{t_1}^{t_2} (I) dt - \Delta n_{O_2}^{gas\ phase} \right) \quad (26)$$

The conductivity of the samples can be measured independently of the surface area with the 4-probe ‘Van der Pauw’ technique.

A bar shaped sample is the most common sample shape for applying the ‘Van der Pauw’ technique. However, it can be difficult to construct a bar with a constant cross section surface of the length of the bar. The ‘Van der Pauw’ technique can also be applied on disc shape samples.

The condition for the ‘Van der Pauw’ method [14]:

1. The sample is of uniform thickness
2. The contacts are at the circumference of the sample
3. The contacts are sufficiently small
4. The surface of the sample is singly connected, i.e.: the sample should be homogenous and should not contain isolated holes.

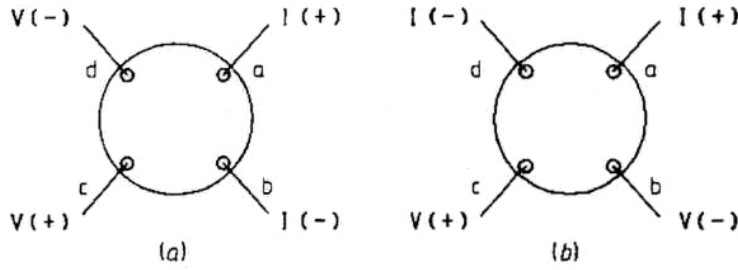


Figure 3: Schematic diagram ‘Van der Pauw’ technique to study the conductivity [14]. Method (a) and (b).

For each conductivity calculation, two resistance must be measured, see (a) and (b) in Figure 3. The electrodes are drawn on the sample, however the electrodes are in practise on the side of the disc shape sample. The resistance $R_{ab,cd}$ is defined as the potential difference between the contacts ‘d’ and ‘c’ per unit current through the contacts ‘a’ and ‘b’. For each measurement the resistance is determined of (R1) $R_{ab,cd} (=V_{cd}/I_{ab}, ‘a’)$ and (R2) $R_{ad,cb} (=V_{cb}/I_{ad}, ‘b’)$, see Figure 3.

The reciprocal of the conductivity is the resistivity ‘ ρ ’. The resistivity [$\Omega \cdot m$] is a function of the thickness (d) and two resistances ($R_{ab,cd}$ and $R_{ad,cb}$), see equation (27).

$$\rho = \left(\frac{\pi d}{\ln 2} \right) \left[\frac{(R_{ab,cd} + R_{ad,cb})}{2} \right] f(R_{ab,cd}, R_{ad,cb}) \quad (27)$$

Whereas the function of the resistances is given as:

$$f(R_{ab,cd}, R_{ad,cb}) \approx 1 - \left[\frac{(R_{ab,cd} - R_{ad,cb})}{(R_{ab,cd} + R_{ad,cb})} \right]^2 - \left[\frac{(R_{ab,cd} - R_{ad,cb})}{(R_{ab,cd} + R_{ad,cb})} \right]^4 \times \left[\frac{(\ln 2)^2}{4} - \frac{(\ln 2)^3}{12} \right] \quad (28)$$

The conductivity can also be measured by using an alternative current (AC) instead of DC measurements described above. The resistance, and the conductivity, can be determined by the impedance at different frequencies by using the software program Equivalent circuit [15]. This technique is called impedance spectrometry and is also able to distinguish the bulk and grain boundary resistance.

3. Existing coulometric titration set-ups

3.1. Oxygen pump and sensor design

In many studies [16-26], a single electrochemical cell is used to measure and control the oxygen partial pressure. Bakken [5] reported that a single cell caused drifts in the EMF if the atmosphere contains a lower oxygen partial pressure than $1 \cdot 10^{-5}$ atm. Bakken [5] avoided the EMF drifts by using a double electrochemical cell with 4 electrodes and obtained a stable EMF at lower oxygen partial pressure ($1 \cdot 10^{-20}$ atm). Other research groups [27-32] used a double electrochemical cell with only three electrodes.

A disadvantage of the three-electrode system is that polarization losses changes too much at the electrode in the reducing environment after a potential steps [4]. The polarization losses exert a significant influence on the accuracy of the oxygen sensor [33]. A 4-electrode system minimises the polarization losses and is used by many research groups [4, 7, 11, 32, 34-53]. A coulometric titration set-up with two separated electrolyte tubes or electrolyte discs with both two electrodes is found also. The four electrodes can also be placed on a single electrolyte. However, the electrodes of the pump and the electrodes of the sensor on the same electrolyte must have a certain distance to avoid interaction.

The choice of on electrolyte is dependent on the requirements of the temperature and oxygen partial pressure. Cubic stabilised zirconia is a pure ionic conductor at temperatures ranging from 800 to 1400 K [10]. The most commonly used electrolyte at this temperature is yttria-stabilised zirconia. The yttria content varies between 3 to 10 mol% for respectively high strength and high ionic conductivity and relative high ionic and stable conductivity. Gadolinium stabilised ceria is an alternative electrolyte at lower temperatures.

The electrolyte must have a certain *thickness* to remain gastight and to have enough mechanical strength. A decrease of the thickness of the electrolyte increases the oxygen ion current. A thinner electrolyte with the same potential results in a higher potential over a short depth and that can result in decomposition. The high potential is also called the decomposition potential 'U'. Schober et al. [54] reported a decomposition potential of 1.2 V for 8YSZ (8 mol% yttria). The decomposition potential 'U' is given by:

$$\Delta_f G = -nFU' \quad (29)$$

Ochin et al. [26] reported a similar value (less than 1.5 V) for preventing reduction of the zirconia tube.

The choice on electrode material is dependent on the temperature. Platinum is the most common used electrode material for metal oxides at high temperature (in the order of 1200 K). The platinum should be porous and clean [7] to obtain fast surface reaction.

Table 1: Overview of samples, limitations of oxygen partial pressure and temperature, number of electrodes and types of measurements performed for all the coulometric titration set-ups found in literature.

Research group	Temp in K	Lowest pO_2 in atm	# electrodes	Sample ¹	Measurement 'δ' non-stoichiometry and 'D' Chemical diffusion, 'σ' conductivity
[4]	973-1273	10^{-4}	3,4	La(Sr)CoO, La(Sr)FeO	'δ'
[16-18]	950-1300	10^{-9}	2	La(Sr)MnO, Sr(Fe)CoO	D, δ
[34]	1073-1273	10^{-16}	4	SrTi(Nb)O	'σ'
[28, 29]	1173-1273	10^{-6}	3	CaTi(Fe)O	'δ'
[19]	950-1300	10^{-5}	2	CaTi(Fe)O	'δ'
[21, 22]	650-1250	10^{-7}	2	BiV(Cu)O, Sr(Fe)CoO	'δ'
[30, 31]	1073-1373	10^{-18}	3	LaMnO, La(Sr)MnO, LaSr(Fe)MnO, LaCrO	'δ'
[35]	1173-1523	10^{-12}	4	Fe(Y)O	'δ'
[11, 36-40]	550-1250	-	4	Gd(Mn)TiO, CuO	'δ'
[55]	1073-1273	10^{-20}	3	Ce(Ca)O, Ce(Gd)O	'δ'
[41-44]	973-1123	10^{-23}	4	Ni-Cr, Fe, Zr, Ti, Ni, Cu, Fe, Mo, Cr	'δ'
[23-25]	673-1273	10^{-20}	2	La(Sr)FeO, La(Sr)MnO, CuO	'δ'
[20]	923-1173	10^{-4}	2	La(Sr)CoO	D, 'σ'
[32]	863-1173	10^{-7}	4	HoBaCuO	'σ', δ
[7, 56]	973-1273	10^{-20}	4	SrTiO	'σ', δ
[5]	1223-1373	10^{-12}	4	SrFeO and CaMnO	'δ'
[27]	1473	10^{-12}	3	Ni, Co, Fe, CoFeO	'δ'
[45-53]	473-1223	10^{-12}	4	Miscellaneous	'σ'
[26]	873-1373	10^{-12}	2	CuO	'σ'

¹ The studied samples are named by the material, the doping content are written between brackets, the stoichiometry is not given. The complete names of the materials are in appendix A 'coulometric titration set-ups'.

3.2. Similarities and differences in coulometric titration set-ups

The coulometric titration set-ups found in literature can be divided into two groups based on the gas volume in the cell. Many set-ups [4, 12, 16-18, 21, 22, 28, 29, 32, 34, 57-61] are designed to minimise the gas volume and thereby to measure the non-stoichiometry accurately. The sample is either directly attached on the electrolyte or the sample is placed in an electrolyte crucible, which is sealed and filled to reduce the gas volume. The volume of the cell is similar to the volume of the sample. The mass of the samples measured by this group varies between 0.04 to 0.7 grams. The second group [7, 11, 23, 24, 26, 27, 35-53, 56, 62-67] contains a gas volume between 7 and 190 cm³ and are listed in Table 2. The mass of the samples measured by the second group varies between 0.3 to 15 grams.

The conductivity and / or the non-stoichiometry of the samples are measured either in argon or in reactive gasses. Sockel et al. [27] and Ohly [7] used hydrogen as reactive gas in their

cells. Mitberg et al. [45-48] controlled the oxygen partial pressure with an initial carbon dioxide/oxygen (50/50) environment and Porat and co-workers [11, 36-40] used argon, carbon dioxide and hydrogen in their cells. Both reactive gases have the disadvantage of possible reactions with the studied material. Hydrogen gas contains always oxygen and water (vapour), whereas carbon monoxide can react to form carbonates.

The oxygen leakage of coulometric titration set-ups is an important factor how the cell performs. Marques et al. [6] found a negligible oxygen leakage through an electrolyte in an oxygen partial pressure range between 10^{-30} and 10^{10} atm. Belzner et al. [16] found a steady state leakage current into their coulometric titration cell ranging from 0.1 to 4 μA and is mostly dependent on the temperature (973 to 1133 K). The oxygen leakage caused by the semi-permeability of the YSZ is dependent on the electrode area. The electrode area of the electrochemical cell in the design of Belzner et al. [16] is 0.2 cm^2 , which results in a specific oxygen leakage of $0.1 \mu\text{A}/\text{cm}^2$ ($0.5 \mu\text{A}$) The coulometric titration set-up of Bakken [5] has a specific oxygen leakage of $40\text{-}400 \mu\text{A}/\text{cm}^2$ (1223 to 1323 K) ($200 \mu\text{A}$).

The current obtained to pump oxygen in or out the cell electrochemically varied between 10 μA to 10 mA. The materials used in coulometric titration set-ups are: stabilised zirconia as electrolyte material, platinum as electrodes and wires, alumina and quartz as inert and insulation material. Brass fittings are commonly based on light metals. The connections between a brass fitting, alumina, electrolyte material and quartz are sealed gas tight with minimal two O-rings, preferable Viton O-rings. Wires are sealed usually with an epoxy resin such as ‘Torr seal’ or a glassy material.

Table 2: Cell volumes of coulometric titration set-ups found in literature.

Research group	Cell volume in cm^3
Socket et al. [27]	7-10
Piekarzcyk et al. [35]	25
Porat and co-workers [11, 36-40]	50
Mizusaki et al. [23-25]	25
Li et al. [41-44]	40
Ohly et al. [7, 56]	80
Mitberg et al. [45-53]	125
Ochin et al. [26]	190

3.3. Problems and challenges in coulometric titration

Iwase et al. [10] reported the possibility of ultra low oxygen partial pressure of $1 \cdot 10^{-25}$ atm. Only a few research groups [7, 30, 41, 45, 59] obtained an oxygen partial pressure in that order. The accessible range of oxygen partial pressure in coulometric titration set-ups is mainly limited by the lowest oxygen partial pressure and is controlled by the oxygen leakage due to oxygen leakage through the sealings (mechanical leakage) and the semi-permeability of the electrolyte material.

Oxygen leakage through the electrolyte can be minimised by cooling the part of the electrolyte that is not used for pumping or measuring the oxygen. The conductivity in solid state electrolytes is generally low at low temperature (800 K) [33].

The working temperature of the electrolyte mainly determines the accessible range of temperature in coulometric titration set-ups. The working temperature of the electrolyte is the temperature whereas the ionic conductivity is high and the electronic conductivity is negligible. The design of e.g. Porat et al. [11] is able to control the temperature of the sample independently of the temperature of the electrolyte. The temperature range is in their set-up only restricted by the material choice of the coulometric titration set-up such as the seal material.

Blackening

The demanding oxygen flux is achieved by applying a potential over the oxygen pump. High potential difference between the electrodes can cause a negative side effect and is called blackening. Blackening occurs when the oxygen vacancies and electrons form clusters. This problem can be avoided by applying small potential steps. So, only small amount of current is transported. However, small potential steps with result in low pump speeds.

4. Defect chemistry of mixed conducting perovskites

4.1. Lanthanum based perovskites

$\text{La}_{1-x}\text{A}_x\text{MO}_{3-\delta}$ (A is Ca, Sr or Ba, M is Cr, Mn, Fe, Co etc.) are mixed ionic and electronic conductors. These materials are of special interest for catalysts, chemical sensors, oxygen separation membranes, SOFCs and other fields. These perovskite type oxide have the characteristics of mixed valence state of the B-site metals (perovskite ABO_3), large non-stoichiometry and formation of solid solutions [23].

The oxygen permeability of lanthanum ferrate perovskites is moderate. The lanthanum ferrate perovskites are stable in strong reducing environments: $1 \cdot 10^{-17}$ atm [9]. The conductivity of $\text{La}_{1-x}\text{Sr}_x\text{FeO}_{3-\delta}$ has been studied at different oxygen partial pressures, different temperatures [68]. The defectchemistry model of $\text{La}_{1-x}\text{Sr}_x\text{FeO}_{3-\delta}$ is described with the Kröger-Vink notation [69], see Table 3.

Table 3: Kröger-Vink notation

Symbol	Explanation
V	Element symbol
..	Net double positive charge with respect to the 'neutral' lattice
'	Net single negative charge with respect to the 'neutral' lattice
x	No charge with respect to the 'neutral' lattice
O	Lattice site

SrFeO_3 is incorporated in LaFeO_3 by the formation of Fe^{4+} cations:



Where, the Sr'_{La} is a Sr^{2+} cation at the La^{3+} lattice site, and $\text{Fe}^{\bullet}_{\text{Fe}}$ is a Fe^{4+} cation on a Fe^{3+} lattice position. The $\text{O}^{\times}_{\text{O}}$ is an O^{2-} on a regular site in the perovskite structure. The non-stoichiometry is in equilibrium with the oxygen partial pressure and can be described as:



The Fe^{4+} cations are reduced to Fe^{3+} ($\text{Fe}^{\times}_{\text{Fe}}$) and the oxygen vacancies ($\text{V}_0^{\bullet\bullet}$) are formed at low oxygen partial pressures. For the sake of simplicity the oxygen vacancies are assumed to be double charged $\text{V}_0^{\bullet\bullet}$. The iron cations concentration is related via the charge disproportionation equilibrium:



The equilibrium constants of the non-stoichiometry reaction (K_{ox}) and the disproportionation reaction (K_{p}) are described as:

$$K_p = \frac{[\text{Fe}_{\text{Fe}}^{\bullet}][\text{Fe}'_{\text{Fe}}]}{[\text{Fe}_{\text{Fe}}^{\times}]^2} \quad (33)$$

$$K_{ox} = \frac{[\text{Fe}_{\text{Fe}}^{\times}]^2[\text{V}_{\text{O}}^{\bullet\bullet}][pO_2]^{1/2}}{[\text{Fe}_{\text{Fe}}^{\bullet}]^2[\text{O}_{\text{O}}^{\times}]} \quad (34)$$

The overall electroneutrality condition can be written as:

$$[\text{Fe}_{\text{Fe}}^{\bullet}] + 2[\text{V}_{\text{O}}^{\bullet\bullet}] = [\text{Sr}'_{\text{La}}] + [\text{Fe}'_{\text{Fe}}] \quad (35)$$

Other defects and sites are in balance with the following conditions:

$$\begin{aligned} [\text{Fe}_{\text{Fe}}^{\times}] + [\text{Fe}_{\text{Fe}}^{\bullet}] + [\text{Fe}'_{\text{Fe}}] &= 1 \\ [\text{La}_{\text{La}}^{\times}] + [\text{Sr}'_{\text{La}}] &= 1 \\ [\text{O}_{\text{O}}^{\times}] + [\text{V}_{\text{O}}^{\bullet\bullet}] &= 3 \end{aligned} \quad (36)$$

The $\text{Fe}_{\text{Fe}}^{\bullet}$ is equal to the amount of electrons and $\text{Fe}_{\text{Fe}}^{\times}$ (Fe^{2+}) is equal to the amount of electron holes. The oxygen vacancy concentration ($\text{V}_{\text{O}}^{\bullet\bullet}$) is the non-stoichiometry term (δ). The equilibrium oxygen partial pressure can now be calculated as a function of the mole fraction of the point defects of equations (31) and (32):

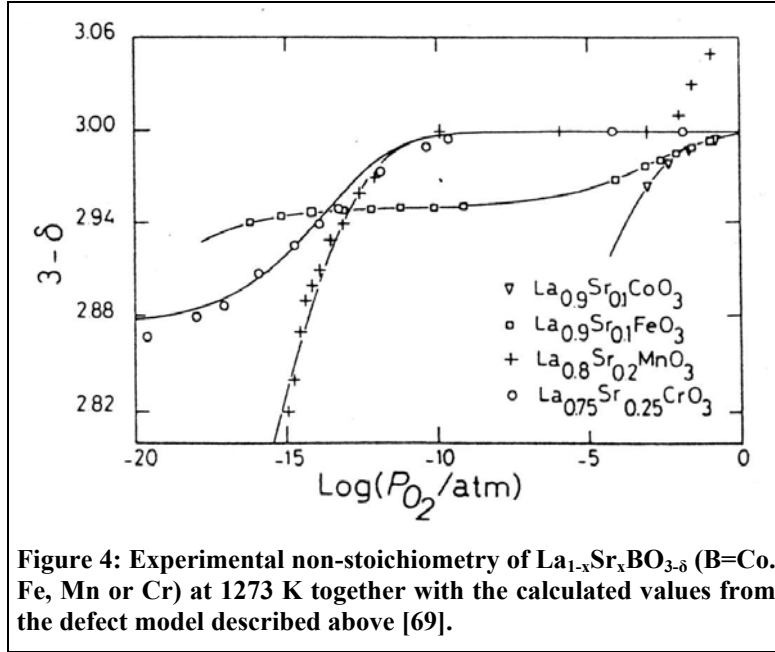
$$p_{O_2} = \left(\frac{K_{ox} K_p [\text{Fe}_{\text{Fe}}^{\bullet}]}{[\text{V}_{\text{O}}^{\bullet\bullet}][\text{Fe}'_{\text{Fe}}]} \right)^2 \quad (37)$$

4.1.1. Non-stoichiometry of $\text{La}_{1-x}\text{Sr}_x\text{FeO}_{3-\delta}$

The non-stoichiometry defined by the defectchemistry model described above is compared with literature results and is presented in Figure 4 with the use of the constants in Table 4.

Table 4: Equilibrium constants of the non-stoichiometry reaction and the proportionation reaction at 1273 K [69].

	$\text{La}_{1-x}\text{Sr}_x\text{FeO}_{3-\delta}$	$\text{La}_{1-x}\text{Sr}_x\text{CoO}_{3-\delta}$
$K_{ox}(\text{atm}^{1/2})$	$7 \cdot 10^{-2}$	$9 \cdot 10^{-3}$
K_p	$1 \cdot 10^{-6}$	$3.5 \cdot 10^{-2}$



The $\text{La}_{1-x}\text{Sr}_x\text{FeO}_{3-\delta}$ material is close to fully oxidised at the highest oxygen partial pressures. There is only a small amount of oxygen vacancies due to the presents of Fe^{4+} which is caused by the strontium doping. The only charged point defects are Sr'_{La} and $\text{Fe}^{\bullet}_{\text{Fe}}$ and the electroneutrality becomes:

$$[\text{Fe}^{\bullet}_{\text{Fe}}] = [\text{Sr}'_{\text{La}}] \quad (38)$$

The concentration of Fe^{4+} is much higher than the oxygen vacancy in the high oxygen partial pressures. Equation (34), reduces to:

$$[\text{V}_\text{O}^{\bullet\bullet}] \propto p\text{O}_2^{-\frac{1}{2}} \quad (39)$$

At lower oxygen partial pressures the amount of oxygen vacancies increases, see equation (34) and the charge compensation occurs via the reduction of Fe^{4+} to Fe^{3+} . Then, the electroneutrality is presented as:

$$[\text{Fe}^{\bullet}_{\text{Fe}}] + 2[\text{V}_\text{O}^{\bullet\bullet}] = [\text{Sr}'_{\text{La}}] \quad (40)$$

No simple relation for the non-stoichiometry can be given. An non-stoichiometry plateau is observed at lower oxygen partial pressures. This region is characterised by the fact that all of the Fe^{4+} have been reduced to Fe^{3+} . The electroneutrality for this region can be written as:

$$2[\text{V}_\text{O}^{\bullet\bullet}] = [\text{Sr}'_{\text{La}}] \quad (41)$$

The oxygen vacancy concentration is stable and equal to the level of strontium doping. At lower oxygen partial pressure, the iron reduces to Fe^{2+} ($\text{Fe}^{\bullet}_{\text{Fe}}$) and finally the material decomposes.

The calculated mole fractions of oxygen vacancy, Fe^{4+} and Fe^{2+} as a function of oxygen partial pressure of $\text{La}_{0.9}\text{Sr}_{0.1}\text{FeO}_{3-\delta}$ is presented in Figure 5.

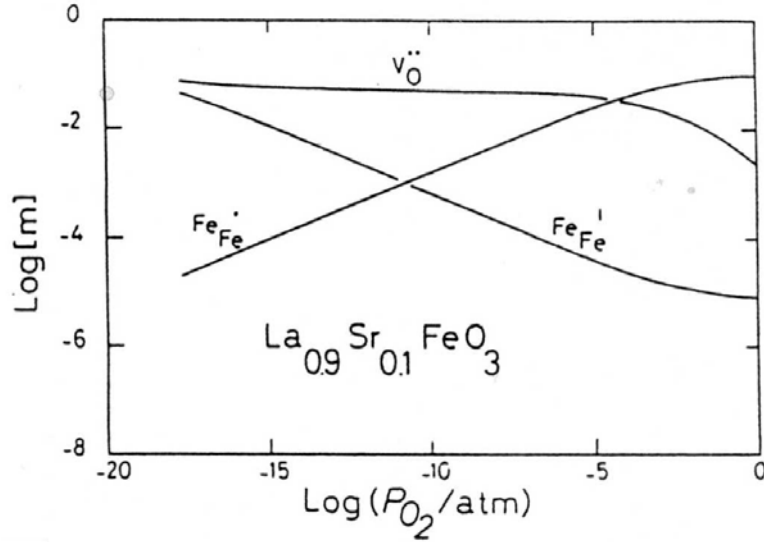


Figure 5: The calculated mole fractions of the oxygen vacancy, Fe^{4+} and Fe^{2+} of $\text{La}_{0.9}\text{Sr}_{0.1}\text{FeO}_{3-\delta}$ as function of the oxygen partial pressure is presented [69].

4.1.2. Conductivity in $\text{La}_{1-x}\text{Sr}_x\text{FeO}_{3-\delta}$

Mizusaki et al. [70] suggested that the electronic conductivity in LaFeO_3 is based on localized electrons. The concentration of the electrons are represented as mole fractions of Fe^{2+} (electrons) and Fe^{4+} (electron holes). The electrical conductivity can be given as:

$$\sigma = \frac{F}{V_M} [u_e n + u_h p] \quad (42)$$

Whereas u_e and u_h are the electric mobilities of the electrons and electron holes. V_M is the molar volume. The concentrations of Fe^{2+} and Fe^{4+} determine the total conductivity, these concentrations are strictly related to the non-stoichiometry as describe above. The total conductivity will have a minimum value when the average oxidation state of iron is three, with the assumption that the mobility of the two species are similar [68].

The charge carriers (in equation (35)) and the mobilities are dependent on temperature. The activation energy of the electron mobility is usually low. The influence of temperature on the mobility is only apparent in the region where the charge carrier concentrations are constant and independent of the temperature. This is the case of high oxygen partial pressure. The conductivity can be given as:

$$\sigma = \frac{F}{V_M} u_h p \quad (43)$$

At lower oxygen partial pressure, the non-stoichiometry is determined by the formation of oxygen vacancies and the reduction of the iron valence. The conductivity decreases with decreasing oxygen partial pressure and increasing temperature. A higher oxygen vacancy concentration and a further reduction of iron to Fe^{2+} at even lower oxygen partial pressure increases the amount of electrons. The conductivity increases with increasing temperature due to the formation of these electrons.

4.2. $\text{La}_{0.95}\text{Sr}_{0.05}\text{CoO}_{3-\delta}$

Lanthanum cobaltates exhibits higher oxygen permeation fluxes than lanthanum ferrates. Therefore, the lanthanum cobaltates are of interest for the above mentioned applications. However, lanthanum cobaltates are not very stable at low oxygen partial pressures [9]. The conductivity of lanthanum cobaltates doped with different strontium content was studied by several groups [4, 20, 71, 72]. The conductivity of $\text{La}_{1-x}\text{Sr}_x\text{CoO}_{3-\delta}$ with a strontium doping of $x=0.05$ has not been studied. In this study the conductivity of a $\text{La}_{0.95}\text{Sr}_{0.05}\text{CoO}_{3-\delta}$ sample is measured at 1065 K in an oxygen partial pressure ranging from air down to the oxygen partial pressure, where the sample decomposes. The defectchemistry model is described in section 4.1. and can be used for $\text{La}_{1-x}\text{Sr}_x\text{CoO}_{3-\delta}$ with some adjustments. Equation (30) becomes:



And equation (31) is rewritten as:



The defectchemistry model is used to calculate the mole fractions of the oxygen vacancies, Co^{2+} and Co^{4+} as function of oxygen partial pressure, see Figure 6. The lanthanum cobaltates show p -type conductivity for all the oxygen partial pressures. Even for large concentration of oxygen vacancies the average valence of the B-site cation (in this case: cobalt) is lower than three. Therefore, the conductivity model described in section 4.1. with charge disproportionation and localised electrons is not applicable for lanthanum cobaltates [68].

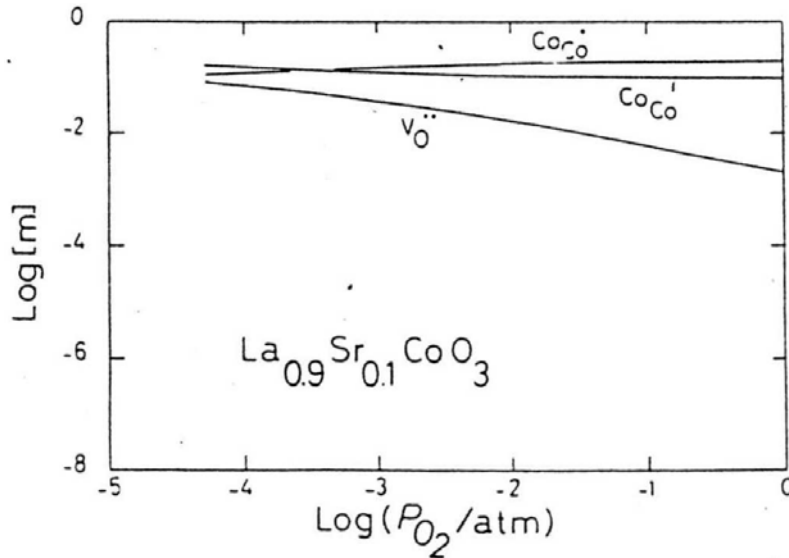


Figure 6: The calculated mole fractions of the oxygen vacancy, Co^{4+} and Co^{2+} of $\text{La}_{0.9}\text{Sr}_{0.1}\text{CoO}_{3-\delta}$ as function of the oxygen partial pressure is presented [69].

The structure of $\text{La}_{1-x}\text{Sr}_x\text{CoO}_{3-\delta}$ is either rhombohedral or cubic, see Figure 7 [71]. The non-stoichiometry of $\text{La}_{1-x}\text{Sr}_x\text{CoO}_{3-\delta}$ increases with decreasing oxygen partial pressure [20, 71, 72]. The electrical conductivity of $\text{La}_{0.9}\text{Sr}_{0.1}\text{CoO}_{3-\delta}$ is $1.6 \cdot 10^3$ S/cm at 973 K in air and $0.5 \cdot 10^3$ S/cm for undoped lanthanum cobaltate. The electrical conductivity of $\text{La}_{1-x}\text{Sr}_x\text{CoO}_{3-\delta}$ increases with strontium content at 973 K with a maximum for $x = 0.4$ [71].

The electrical conductivity of $\text{La}_{1-x}\text{Sr}_x\text{CoO}_{3-\delta}$ is almost independent on the strontium content (0.1-0.3) and is $1.3 \cdot 10^3$ S/cm in air at 1073K. However, the electrical conductivity of undoped lanthanum cobaltate is an order lower than $\text{La}_{0.9}\text{Sr}_{0.1}\text{CoO}_{3-\delta}$ in air at 1073K [71].

The electrical conductivity decreases with decreasing oxygen partial pressure above 800K for a strontium content of 0.3 in the near atmospheric condition [71].

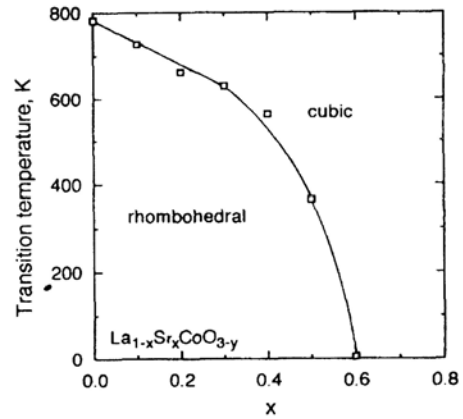


Figure 7: Transition temperature from the rhombohedral to the cubic structure for $\text{La}_{1-x}\text{Sr}_x\text{CoO}_{3-\delta}$ [71].

4.3. $(\text{La}_{0.8}\text{Ca}_{0.2})_{1.01}\text{FeO}_{3-\delta}$

Calcium-doped lanthanum ferrates are also of interest for previously mentioned applications. A patent has been written for $(\text{La}_{0.8}\text{Ca}_{0.2})_{1.01}\text{FeO}_{3-\delta}$ [73]. The defectchemistry model described in section 4.1. for $\text{La}_{1-x}\text{Sr}_x\text{FeO}_{3-\delta}$ can be used to describe the defect chemistry of $(\text{La}_{0.8}\text{Ca}_{0.2})_{1.01}\text{FeO}_{3-\delta}$. Only, equation (30) is different for $(\text{La}_{0.8}\text{Ca}_{0.2})_{1.01}\text{FeO}_{3-\delta}$ and becomes:



5. Experimental

5.1 Sample preparation

$\text{La}_{0.95}\text{Sr}_{0.05}\text{CoO}_{3-\delta}$ and $(\text{La}_{0.8}\text{Ca}_{0.2})_{1.01}\text{FeO}_{3-\delta}$ powders were synthesized by the EDTA-route as reported by van Doorn et al. [74]. The powders are pressed uniaxially (28 MPa for five minutes) in a mould to form a disc-shaped sample. The density of the samples is increased by isostatic pressure (400 MPa for five minutes). The $\text{La}_{0.95}\text{Sr}_{0.05}\text{CoO}_{3-\delta}$ sample is sintered at 1150°C for 10 hours and $(\text{La}_{0.8}\text{Ca}_{0.2})_{1.01}\text{FeO}_{3-\delta}$ sample is sintered at 1300°C for 10 hours, the heating and cooling rate was set at 1°C/min. The samples (\varnothing 15mm, thickness \pm 1mm) are grinded with a diamond paste of 3 μm .

5.2 Design of the coulometric titration set-up

The coulometric titration set-up of this study is designed to control the oxygen partial pressure between 1 and $1 \cdot 10^{-15}$ atm. in a temperature window of 600 to 1000°C.

The set-up is designed with the following requirements:

- Easy sample change
- Easy change of gas condition
- Oxygen sensor independent of the oxygen pump
- Conductivity measurements by ‘Van der Pauw’ technique

The design is a static gas system with a single electrolyte material with a double electrochemical cell. The electrolyte material is an YSZ tube (205x13 \varnothing_{out} mm) based on the available material, produced by Gimex, Geldermalsen, The Netherlands. The cell, oxygen sensor / pump, sealing, sample holder, gas system and the electrical equipment of this design are discussed below.

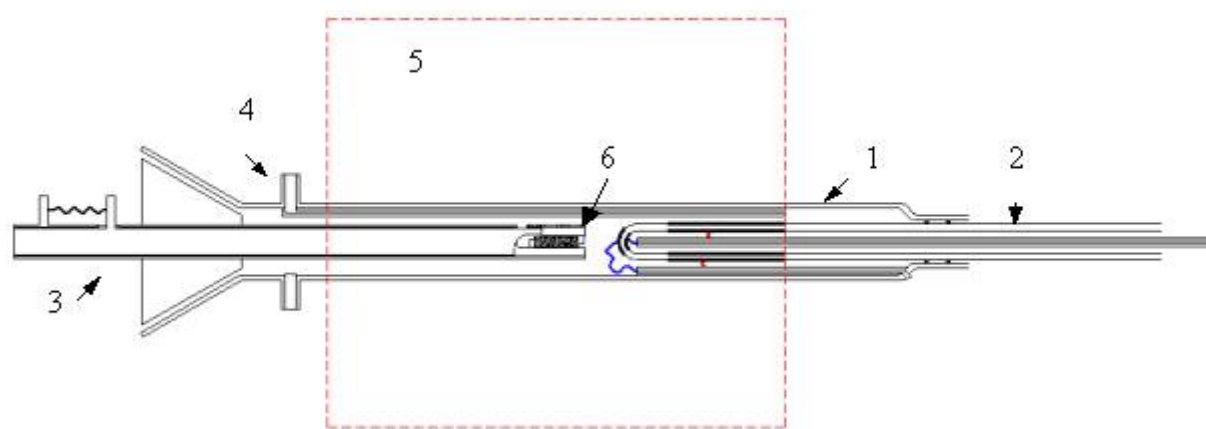


Figure 8: Schematic overview of the coulometric titration design of this work. A quartz tube (1) with a gas inlet (4) is located in a tubular furnace (5). A sample holder (3) with sample (6) is inserted on the left of the quartz tube. A YSZ tube (2) acting as a double electrochemical cell (oxygen sensor at the tip of the YSZ tube and an oxygen pump) is inserted on the right side of the quartz tube.

5.2.1 Cell

The cell, with a volume of 0.14 l, contains the oxygen sensor / pump, sample holder and a sample. The allowed sample size is between 8 and 18mm in diameter and a maximum thickness of 3 mm. The cell is inserted in a tubular furnace (27 mm \varnothing X 160 mm long). The material of the cell has the following requirements: The cell must be gastight, withstand high

temperature gradients, insulate temperature and must be sufficient mechanically strong. Quartz and alumina are two possible materials for the use of coulometric titration cell. Quartz crystallises. However, quartz material is easy to adjust in certain shapes.

The size of the furnace is determined by the size of the cell. The length and the diameter of the cell are as small as possible to minimise the gas content. And thereby, the equilibration time to obtain stable oxygen partial pressure is minimised.

The temperature of the tubular furnace is controlled with an accuracy of 0.1 K. The temperature profile is recorded and the temperature is constant ($\pm 4\text{K}$) over a distance of 30 mm in the centre of the furnace.

5.2.2. Oxygen sensor and pump

The oxygen sensor is located as near as possible to the sample. The oxygen pump and the oxygen sensor are applied on the same electrolyte material to simplify the set-up, see Figure 9. The oxygen sensor and pump are at a distance of 20 mm from each other to avoid interaction.

The YSZ tube, is painted with 'Comptoir Lyon Alemand Louyot Platinum-paste L42' electrodes with a paintbrush. The platinum paint is fired (1323 K for 2 hours with a rate of 2 K/min). A porous platinum layer is observed with a light microscope. The porous layer benefits the oxygen exchange with the surrounding and the YSZ-tube. The sensor area is equal to the tip of the tube and corresponds to an area of 1 cm^2 . The pump electrode area (5 cm^2) is located at a distance of 20 mm of the sensor to avoid interaction of these electrodes. The pump electrode is painted around the tube over a distance of 40 mm, to obtain a large surface exchange area.



Figure 9: Picture of oxygen sensor and pump in quartz tube.

The electrodes inside the YSZ-tube are painted similarly. The inside of the tube is painted by turning the YSZ tube around a paintbrush. The YSZ-tube is placed into a furnace over a length of 70 mm. The maximum temperature at the flanges is about 800 K with a temperature in the middle of the furnace of 1200 K. The temperature of the YSZ tube at the flanges controls the length of the pump electrodes due to the working temperature of the YSZ-tube.

A platinum wire ($\varnothing 0.2\text{ mm}$) is wound around a quartz ring, see Figure 9. The YSZ tube is inserted in this ring and the weight of the ring proved to be enough to maintain contact between the outer pump electrode and the wire. A second ring was held in position by the cell wall and the tip of YSZ-tube was spring loaded against this second ring. The spring is connected with the quartz tube and attached to the YSZ-tube and is located outside the furnace. Resistance over the sensor and pump electrodes are obtained in the order of several Ohms ($2\text{-}200\Omega$) in air at 1100 K.

The connection of the inner sensor electrode is achieved with a platinum gauze. The platinum gauze is attached on an alumina tube, which contains four capillaries. This alumina tube is spring loaded (outside the furnace) to maintain contact between the inner sensor electrode and the platinum gauze. One of the capillaries insulated a platinum oxide wire that connects the platinum gauze. A second platinum wire is in one of the other capillaries and connects a second platinum gauze wound around the alumina tube. This second platinum gauze is located 30 mm distance of the tip of YSZ-tube, the weight of the alumina tube and the size of the platinum gauze results in good contacts with low electrical resistance.

5.2.3. Sample holder

The sample holder consist four electrodes that maintain contact with the sample, see Figure 11. The four electrodes are made of platinum thin film and are connected with a platinum wire. Two electrodes are fixed on the sample holder and a second pair of electrodes is spring loaded to insure contact between electrodes and samples. The spring is located outside the furnace.

The sample holder is connected with the cell via a quartz glass joint. Grease is used in the quartz connection to obtain a gastight sealing.

The sample holder carries also a thermocouple to monitor the temperature at the sample. The thermocouple is based on a platinum wire connected with a 10% rhodium doped platinum wire. In summary, the sample holder transports 6 wires from near the sample to the outside of the furnace. These wires were insulated with quartz capillaries (\varnothing_{in} 0.5 mm). The quartz capillaries are open near the sample and sealed gastight with ‘Torr seal’ outside the furnace.

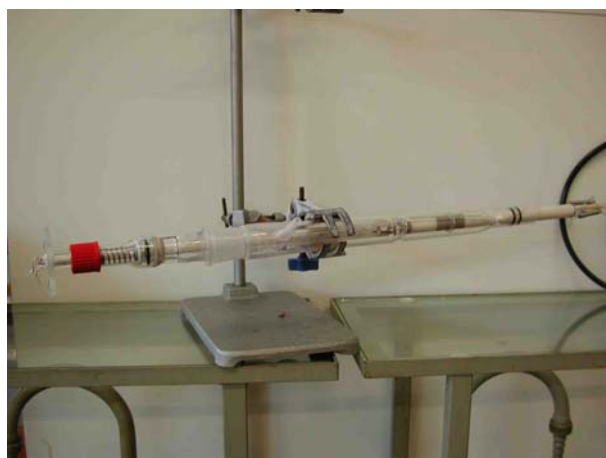


Figure 10: Overview cell with inserted sample holder (left) and oxygen sensor and pump (right) in the quartz tube. The red screw cap holds the spring in position. The spring pulls on the inner quartz tube, see Figure 11



Figure 11: Sample holder tip with 4 electrodes. The inner quartz tube is pressed slightly, with the spring, to the left. The two electrodes on the right are connected on the inner quartz tube. These two electrodes press the 1 euro cent against the other two electrodes that are fixed on the outer quartz tube.

5.2.4. Sealing

The quartz tube and YSZ tube were connected gastight with the use of two Viton O-rings. The outer electrodes (located in the quartz tube) were connected with platinum wires. These wires must be transported out of the cell to enable a connection to the electrical equipment. The transportation to the outside the quartz tube can only be sealed gastight in the cold parts with sealants such as ‘Torr seal’.

5.2.5. Gas system

The cell can be flushed with different gases, see Figure 12. The gas in and outlet tubes are connected with metal connectors. The gas supply is controlled and monitored with mass flow controllers. The outlet gas is fed to the vent. The used gases are: technical air, argon (oxygen partial pressure of $1 \cdot 10^{-5}$ atm.) and 50 ppm CO_2 in nitrogen (oxygen partial pressure of $1 \cdot 10^{-4}$ atm.). The cell can be emptied with the use of a vacuum pump. The cell is emptied and filled at least three times (until similar oxygen partial pressure is obtained). The oxygen leakage is minimised by filling the cell with an overpressure of several mbar, measured with a separate barometer. The gas outlet of the vacuum pump is led to the vent.

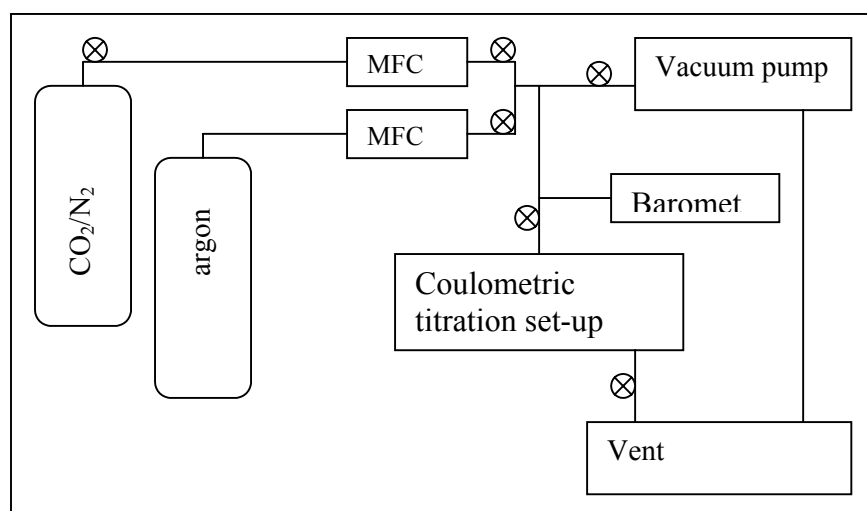


Figure 12: Schematic overview of the gas system. The gases are controlled with (MFC) mass flow controllers. The figures (⊗) are valves. The cell can be emptied with a vacuum pump and the total pressure can be determined with a barometer.

5.2.6. Electrical equipment

Oxygen sensor / pump

The oxygen sensor is monitored with a Keithley 617 electrometer and registered with an Ankersmit A41 recorder. The oxygen pump is connected with a Bank Potentiostat MP 81 to control the potential over the pump and to measure the current. The current output of the potentiostat is a potential and can be calculated to the actual current by dividing the potential with a 109.4Ω parallel-connected resistance, the potential is recorded. The pump current is used to calculate the amount of oxygen pumped in or out.

Conductivity

A Philips power supply (PE 4818) applies a minimal potential of 0.65V over the sample, the amount of current is measured with a Keithley 197 multimeter, see Figure 13.

The potential over two opposite electrodes is measured with a second Keithley 197 multimeter. The electrode arrangement is switched to a different ‘sequence’, see Figure 13. The two resistances obtained from both configurations are combined for the calculation of the conductivity, see equation (27).

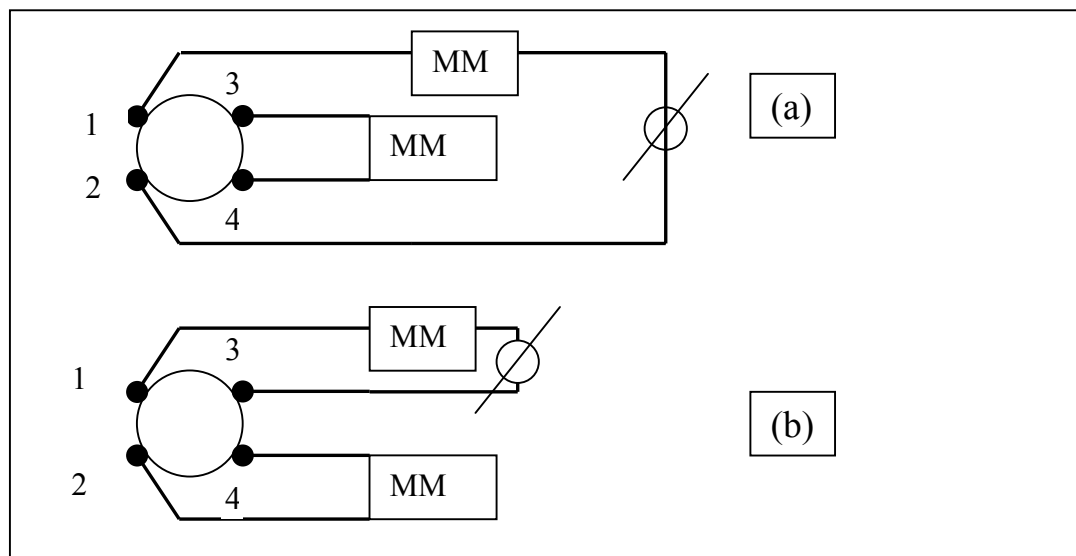


Figure 13: Schematic overview of the electrical circuits and equipments of the ‘Van der Pauw’ conductivity set-up. 1,2,3 and 4 are the four probes. The potential and current is monitored with multimeters (MM). Both configuration methods (a and b) were presented.

5.3. Development of the coulometric titration set-up

The coulometric titration set-up has been modified several times and is presented in Table 5.

Table 5: Code description of Development and type of measurements for the coulometric titration cells. Two YSZ tubes are used (A and B). In total 7 Quartz tubes have been used (0-6). The sample holder has been changed (S1 and S2) twice.

Date	Code	Change	Measurement
12-12	A0S1	First design	Oxygen leakage
08-01	A1S1	Feed-throughs, Pt-gauzes	Oxygen leakage
22-01	A2S1	Smaller inner gas tube	Oxygen leakage and conductivity of $\text{La}_{0.95}\text{Sr}_{0.05}\text{CoO}_{3-\delta}$
13-02	A2S1	Quartz tube cleaned	Oxygen leakage / sorption
14-02	A3S1	Quartz tube, cleaned sample holder	Oxygen leakage / sorption
16-02	B4S1	Quartz tube, YSZ tube, Pt-gauzes	Oxygen leakage / sorption
15-03	A5S1	Quartz tube, cleaned sample holder, wrapping Pt-wire	Oxygen leakage / sorption
19-03	B6S2	Quartz tube, cleaned YSZ, new sample holder	Oxygen leakage and conductivity of $(\text{La}_{0.8}\text{Ca}_{0.2})_{1.01}\text{FeO}_{3-\delta}$

5.3.1. Cell / sealing

The mechanical oxygen leakage of quartz glass joints can be detected by applying a vacuum. The total pressure is stable in case of good sealing of the quartz connection with the use of enough (proper) grease. However, the amount of grease should be reduced to minimise carbon contamination of the cell.

The Viton O-rings oxygen leakage is tested in a similar way as the quartz glass joints. The oxygen leakage in cell A1S1 was not decreased with more Viton O-rings.

In principle, the oxygen leakage due to the semi-permeation of the electrolyte material can be neglected, unless the electrolyte is contaminated. ‘Torr seal’ decomposes at temperatures above $\sim 100^{\circ}\text{C}$ (colour black), then it is not gastight.

The oxygen leakage was observed by a Helium test: The cell is attached to a vacuum system with a mass spectrometer, which has a specific high sensitivity for helium. The outside of the cell is scanned with a local helium flow applied from a helium gas gun.

The helium test results in small (helium) leakage close to the ‘Torr seal’. Small feed-throughs of 40 mm are used to increase the distance between the furnace flange and the position of the seal (A1S1). A second helium test resulted in a similar helium leakage location with less oxygen leakage. The oxygen leakage through the ‘Torr seal’ was minimised by:

- using a syringe to inject liquid ‘Torr seal’ in the feed-through (A2S1)
- cooling the ‘Torr seal’ with flowing air (A2S1).

5.3.2. Oxygen sensor and pump

The connection of the outer sensor electrode and the quartz ring proved to be poor (A0S1). Despite the spring, the YSZ tube is pressed outward due to a slight overpressure in the cell. The connection rings have been replaced by platinum gauzes and are fired (1323 K for 2 hours with a rate of 2 K/min) on the YSZ with platinum paste to obtain permanent connection (A1S1). The oxygen pump electrode area is increased by painting the YSZ tube at a distance of 10 mm from the sensor electrodes. To increase the pump electrode area in the hot zone of the furnace. Therefore, a higher pump speed can be obtained.

The platinum gauzes connected with the outer pump electrode are further simplified by wrapping platinum wire directly around the YSZ-tube (A5S1). The wrapped wire is also fired. The platinum wires connected with the outer sensor and outer pump electrodes obtained no significant electrical resistance.

5.3.3. Sample holder

A stable oxygen partial pressure is observed with flushing the cell with argon in for about 16 hours without sample. A similar equilibration time is observed after an oxygen partial pressure step applied by the oxygen pump without sample (S1).

This equilibration time is mainly determined by (oxygen) gas diffusion in the (dead volume of the) cell. The equilibration time can be reduced by e.g. decreasing the dead volume in the sample holder.

Another sample holder (S2) was designed to minimise the dead volume, see Figure 14 and Figure 15. The sample holder contains a half open tube that carries the platinum wires for the electrodes and the thermocouple. A gastight seal is applied to a 4-bore alumina tube (for the four electrode wires) and a 2-bore alumina tube (for the thermocouple wires) at the sample side using an alkali silicate glass [8436 Schott Glas Mainz, Germany].

The sample is maintained in position and connected with four electrodes. These electrodes are constructed of platinum film and are wound around quartz pins. The pins (arms) are connected to the half open quartz tube at a distance of about 100 mm from the sample, see Figure 14. The benefit of the length of the quartz arms is the elasticity. The space between the electrodes was slightly less than the standard sample size ($\text{Ø} = 15 \text{ mm}$). The elasticity of the arms provides a light pressure on the sample and was proved to be sufficient to maintain contact between electrodes and sample (at high temperature). The dead volume is decreased because of the sealed alumina tube.



Figure 14: Second sample holder (S2) with sample. The arms are connected close to the glass joint. The 4-bore alumina tube (white) is in the middle of the sample holder.

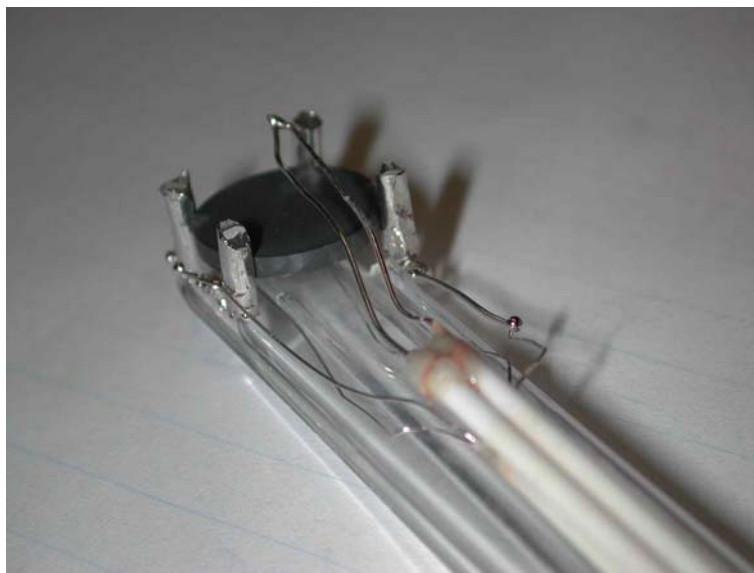


Figure 15, Second sample holder, picture of the sample area. The 4 platinum film electrodes maintain contact with the sample. The electrodes are connected with platinum wires. A 2-bore alumina tube insulated the thermocouple wires. The thermocouple is located above the sample. The sodium silicate is located at the ends of the alumina tubes and is grey.

6. Results

6.1. XRD $(La_{0.8}Ca_{0.2})_{1.01}FeO_{3-\delta}$

The crystal structure of the $(La_{0.8}Ca_{0.2})_{1.01}FeO_{3-\delta}$ powder is analysed using XRD. It appears to be a single phase perovskite with a rhombohedral structure, see Figure 16 and Table 6. The theoretical density of $(La_{0.8}Ca_{0.2})_{1.01}FeO_3$ is 6.22 g/cm^3 . The Rietveld refinement shows a good agreement between the theoretical crystal structure and the structure of the $(La_{0.8}Ca_{0.2})_{1.01}FeO_{3-\delta}$ powder

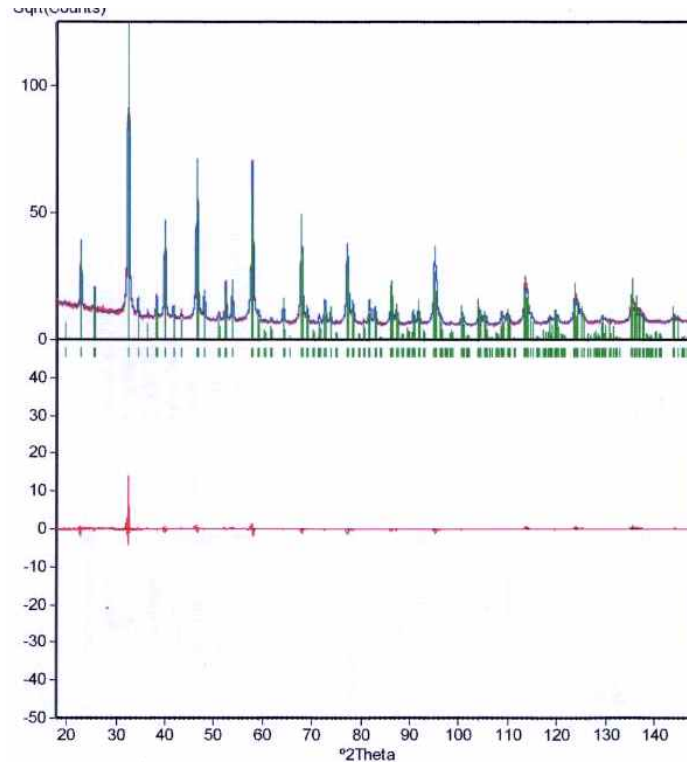


Figure 16: XRD result of $(La_{0.8}Ca_{0.2})_{1.01}FeO_{3-\delta}$ powder. The red line presents the Rietveld refinements. All the peaks at different angles match with the peaks of a single crystal of $(La_{0.8}Ca_{0.2})_{1.01}FeO_{3-\delta}$.

Table 6: Lattice parameters of $(La_{0.8}Ca_{0.2})_{1.01}FeO_{3-\delta}$ (Space group is $Pnma$; rhombohedral structure)

Lattice parameter (error last digit) in Å	
a	5.5264(1)
b	7.8035(2)
c	5.5213(1)

6.2. Oxygen leakage

The performance of the cell can be measured easily by monitoring the oxygen leakage. The cell is flushed with pure argon with only a few parts per million (ppm) of oxygen, which corresponds to an oxygen partial pressure of $\sim 1 \cdot 10^{-5}$ atm or 200 mV potential gradient (OCV at the oxygen sensor, see equation (1)) with air as reference at 1075 K.

The cell is flushed with an argon flow of 50 to 70 ml/min at 938°C, see Figure 17. At first, the cell is flushed with a flow of 50 ml/min argon until a stable oxygen partial pressure is observed. Next, the cell is flushed with a flow of 70 ml/min to obtain a stable oxygen partial pressure. The flushing steps take typically 80 min. Finally, the oxygen leakage is observed after the valves on the cell are closed. The oxygen leakage is measured after each modification of the cell and at different temperatures. The sequence of these measurements is listed in Table 7. The time dependence of the oxygen leakage is presented in Figure 18. The oxygen leakage rates in mol O₂/s for each measurements are presented in Figure 19.

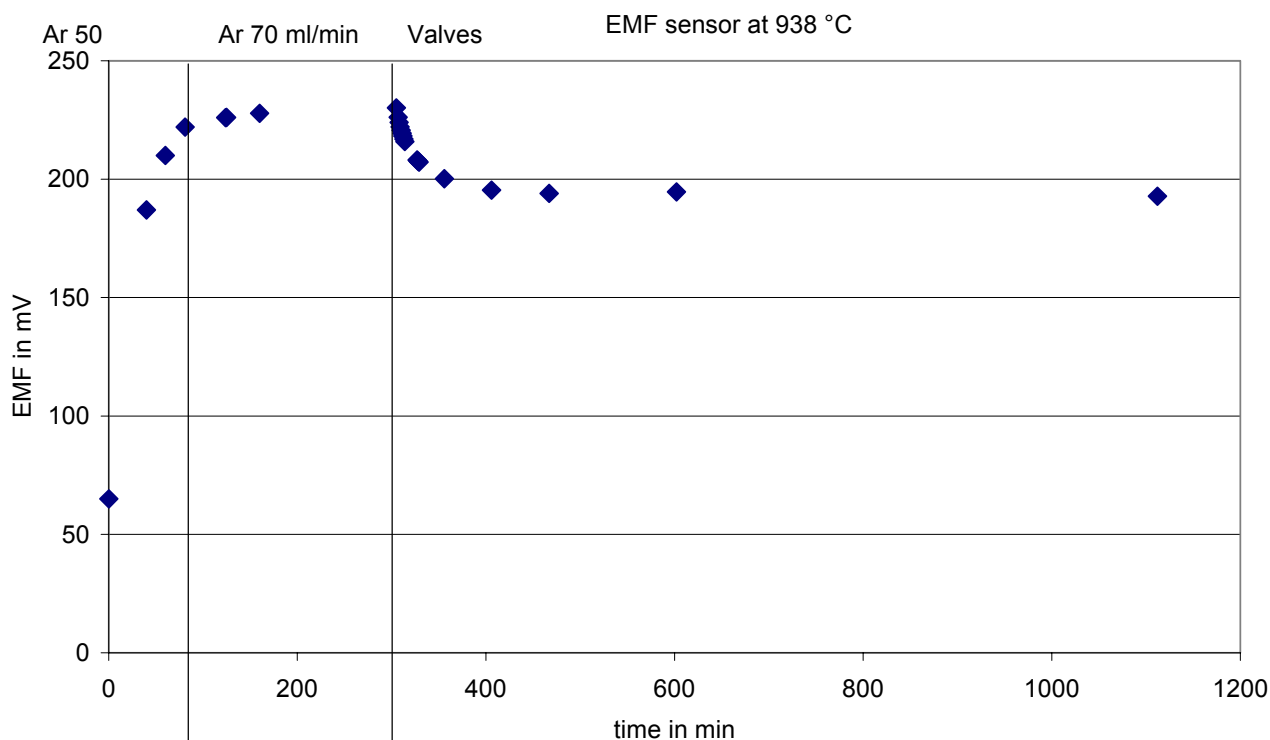


Figure 17: Time dependence of the EMF. At $t=80$ min, the oxygen partial pressure is more or less stable and the argon flow is increased to 70 ml/min. At $t=300$ min, the oxygen partial pressure is stable and subsequently the valves are closed.

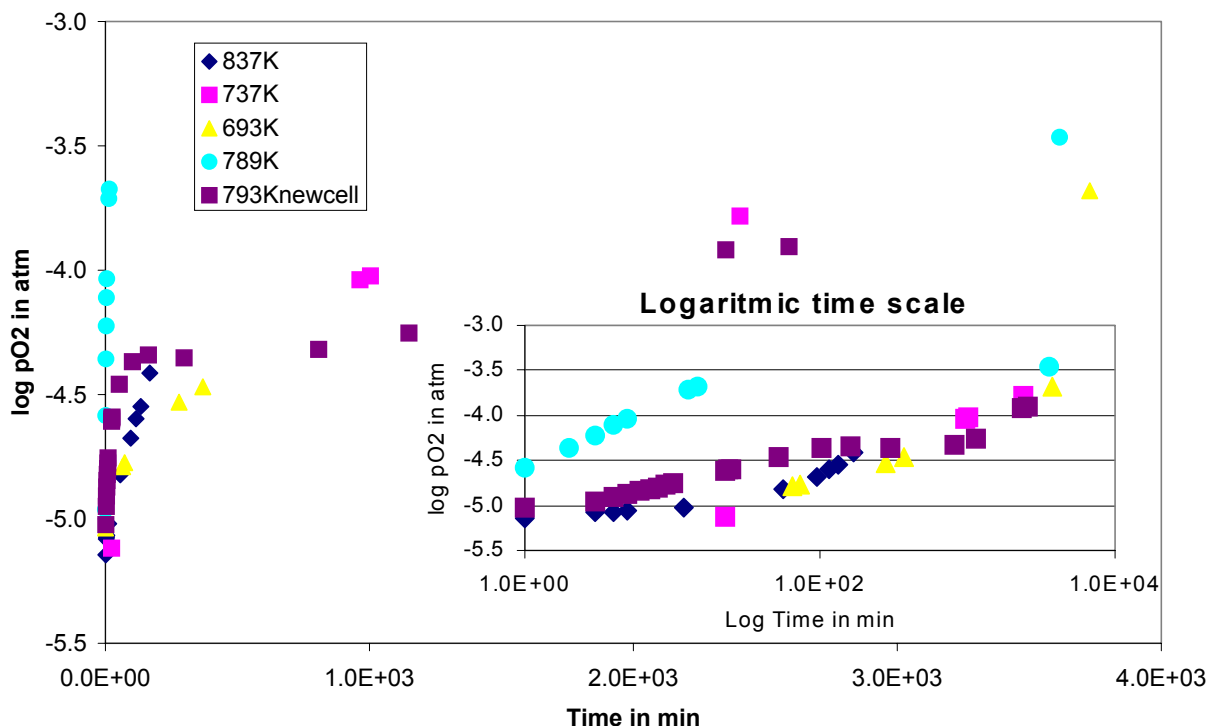


Figure 18: The oxygen partial pressures as function of time presents the oxygen leakage for the different cells (at different temperature), see Table 7. The inset figure is the same oxygen partial pressure versus the logarithmic time scale.

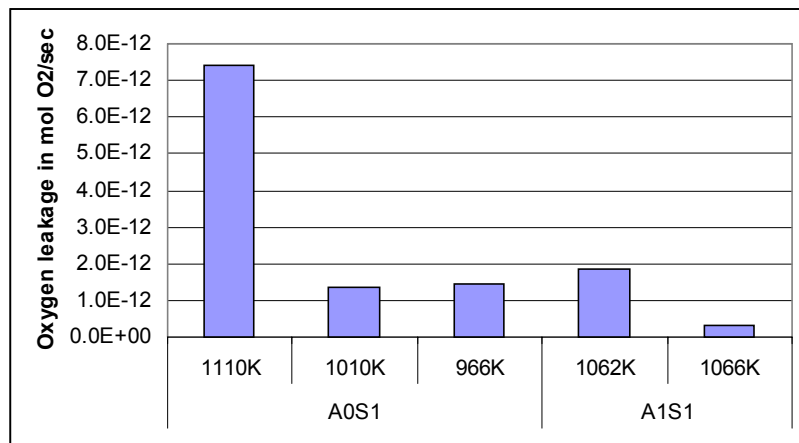


Figure 19: Oxygen leakage rate (in mol O₂/sec) for two modifications of the set-up at different temperatures.

Table 7: Sequence and temperatures of the oxygen leakage measurements

Date	Cell	Temperature
17-12-03	A0S1	1110K
18-12-03	A0S1	1010K
19-12-03	A0S1	966K
09-01-04	A1S1	1062K
12-01-04	A1S1	1066K

Oxygen pump

The oxygen leakage can also be calculated from the amount oxygen that is pumped in or out a constant oxygen partial pressure. The potentiostat is set at a fixed potential over the electrodes of the oxygen pump. The amount of current transported is recorded, see Figure 20. The integrated current is converted to the equivalent of oxygen mol with equation (8). This amount of oxygen molecules is the amount of oxygen pump in or out of the cell. With the assumption that the cell does not react with oxygen.

The final pump current is about 0.1mA and corresponds with $2 \cdot 10^{-10}$ mol O_2 /sec in an oxygen partial pressure in the order of $1 \cdot 10^{-6}$ atm at 792°C . Whereas the oxygen leakage of A1S1 showed an oxygen leakage of $1 \cdot 10^{-12}$ mol O_2 /sec at an oxygen partial pressure of $1 \cdot 10^{-4}$ atm at 792°C . The final pump current presents the oxygen leakage current.

The equilibration time for a stable oxygen partial pressure is in the order of 1000 minutes (16 hours). A typical time dependence of the oxygen partial pressure and the pump current versus time after a potential step of 40 mV over the oxygen pump is presented in Figure 20.

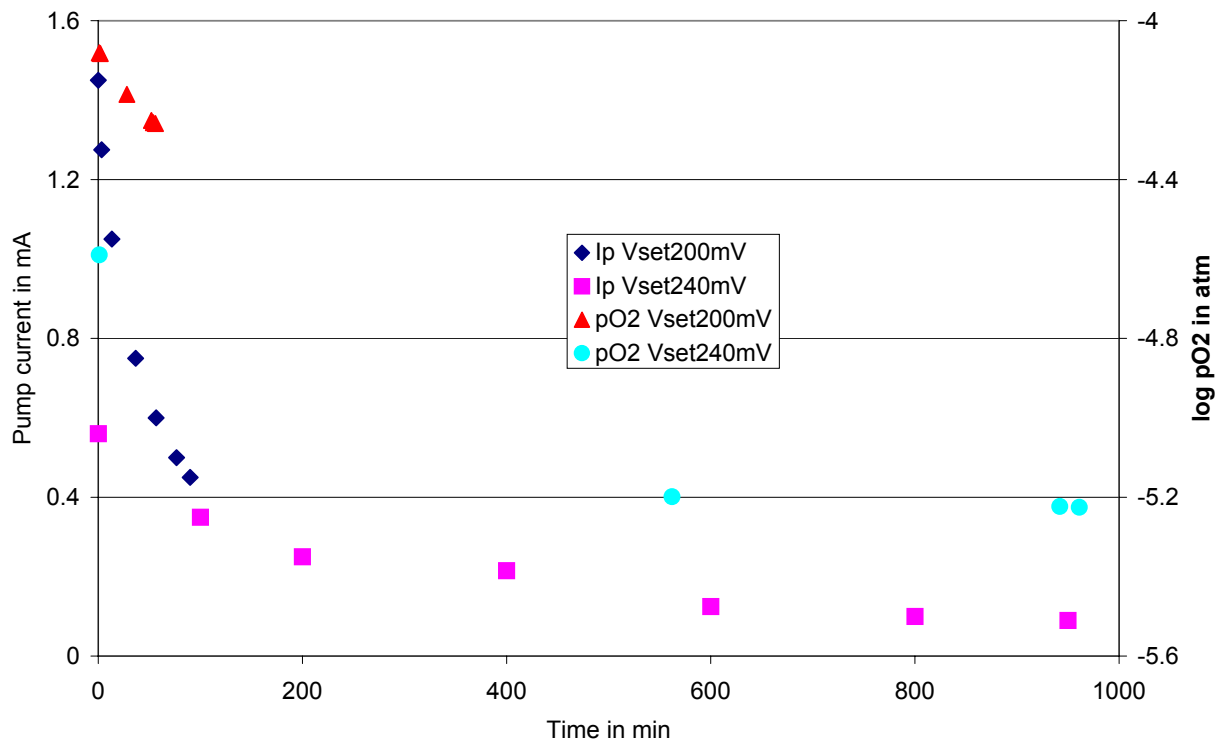


Figure 20: The time dependence of the oxygen partial pressure \blacktriangle and the pump current \blacklozenge is recorded after a potential step of 40 mV to a potential set of 200 mV. A similar time dependence was obtained for a potential step of 40 mV to 240mV. Whereas \blacksquare presents the oxygen partial pressure and \bullet the pump current.

6.3. Oxygen absorption

It was not possible to determine the oxygen leakage after the $\text{La}_{0.95}\text{Sr}_{0.05}\text{CoO}_{3-\delta}$ sample had been studied. The oxygen content in the cell decreased with time instead of increasing due to oxygen leakage in similar environment and temperature. This behaviour was noticed for the cell with and without sample present. A possible cause of the decreasing oxygen partial pressure is the present of a contamination. This contamination is likely originated from the $\text{La}_{0.95}\text{Sr}_{0.05}\text{CoO}_{3-\delta}$ sample. The $\text{La}_{0.95}\text{Sr}_{0.05}\text{CoO}_{3-\delta}$ sample has been in reducing environment and decomposition has been observed.

The absorption time dependence has been monitored and is presented in Figure 21. Both oxygen pump and sensor suggest that the oxygen content decreases even after 3000 minutes (2 days).

Cell A2S1 has been cleaned with nitric acid and ethanol with no success. The quartz tube has been replaced and the sample holder is cleaned with nitric acid and ethanol (A3S1). The oxygen partial pressure of a new cell; new quartz tube and new YSZ tube (with old sample holder) has been measured and the oxygen partial pressure decreased to a typical figure of $5 \cdot 10^{-7}$ atm. Finally, the first YSZ tube (S1) have been polished with a diamond paste of $10 \mu\text{m}$ paper and new electrodes have been painted and fired (as described before). The oxygen leakage has been studied of this cell (A5S1) without sample holder and again an oxygen partial pressure decrease has been observed, see Table 5.

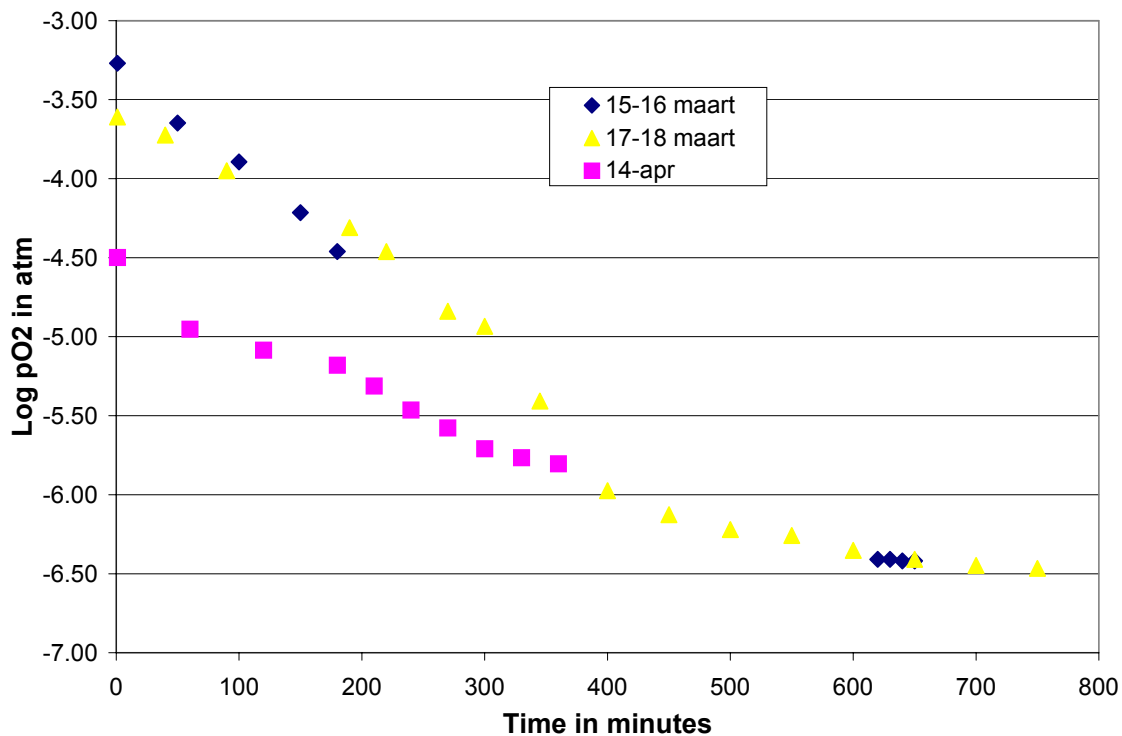


Figure 21: The time dependence of the oxygen partial pressure decrease at 1075 K. The cell has been flushed with argon and sequenced by closing the valves of the cell A5S1 (with a plug instead of the sample holder S1).

6.4. Conductivity

The conductivity has been measured as following the procedures described in chapter 2. The sample holder and / or the sample present an offset potential in both measuring methods (A and B), when no potential is applied. The actual conductivity of $\text{La}_{0.95}\text{Sr}_{0.05}\text{CoO}_{3-\delta}$ is calculated with a corrected potential. A typical linear current potential relation (I-V) to determine the offset potential is presented in Figure 22.

6.4.1. $\text{La}_{0.95}\text{Sr}_{0.05}\text{CoO}_{3-\delta}$

The conductivity of $\text{La}_{0.95}\text{Sr}_{0.05}\text{CoO}_{3-\delta}$ is measured in argon at 1065 K. The presented conductivities are measured in a stable oxygen partial pressure environment. The oxygen partial pressure environment is assumed to be stable when the oxygen pump transports constantly a certain amount of oxygen out of the cell, which corresponds to the oxygen leakage. The obtained equilibration time is 1000 minutes typically. More variation of the conductivity measurements has been observed within the equilibration time of 1000 minutes after a potential step.

The conductivity of $\text{La}_{0.95}\text{Sr}_{0.05}\text{CoO}_{3-\delta}$ sample is stable in an oxygen partial pressure range of $1 \cdot 10^{-6}$ to $1 \cdot 10^{-12}$ atm and is about $1 \cdot 10^3$ S/cm. The $\text{La}_{0.95}\text{Sr}_{0.05}\text{CoO}_{3-\delta}$ sample decomposes in an oxygen partial pressure lower than $1 \cdot 10^{-14}$ atm, see Figure 23. Next, the oxygen partial pressure was increased to study the conductivity of $\text{La}_{0.95}\text{Sr}_{0.05}\text{CoO}_{3-\delta}$ after being in reducing atmosphere. The observed conductivity plateau (similar conductivity at different oxygen partial pressures) has been observed again but with a lower conductivity.

The oxygen leakage was not measured without the sample due to; oxygen leakage variation with various cells and temperature. Therefore, the non-stoichiometry was not able to determine.

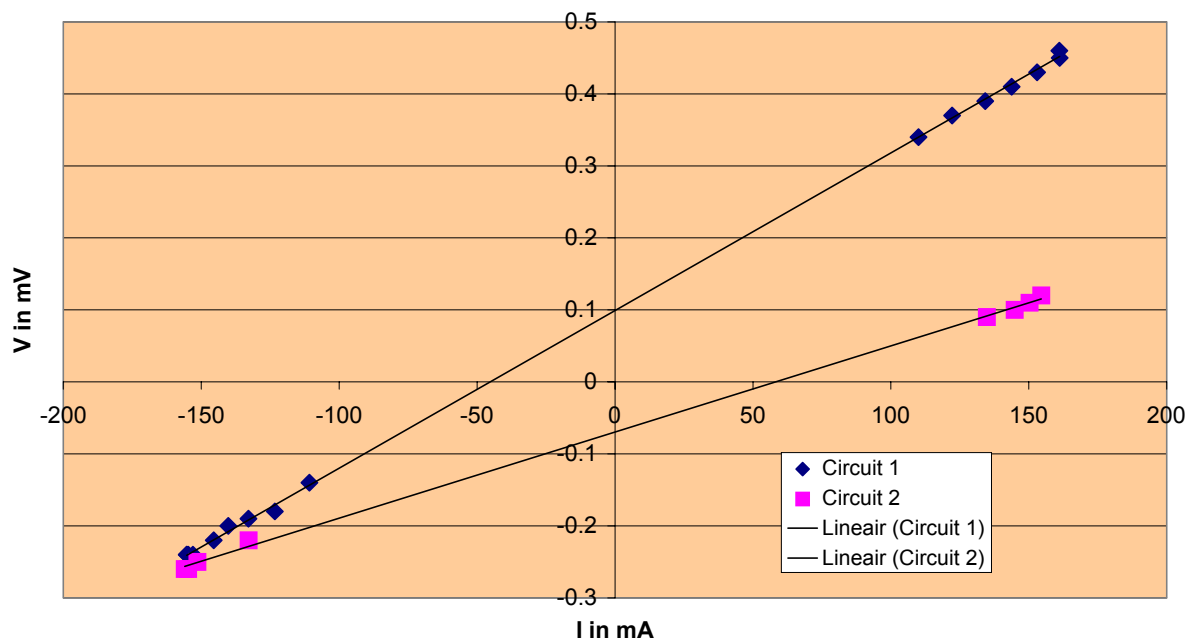


Figure 22: Different potentials are applied on the sample to determine the offset of the sample and sample holder. The applied potential generated a current. This current is plotted versus the potential over the other electrodes. The slopes present the actual R_1 (◇) and R_2 (■), respectively ‘Van der Pauw’ method 1 and 2.

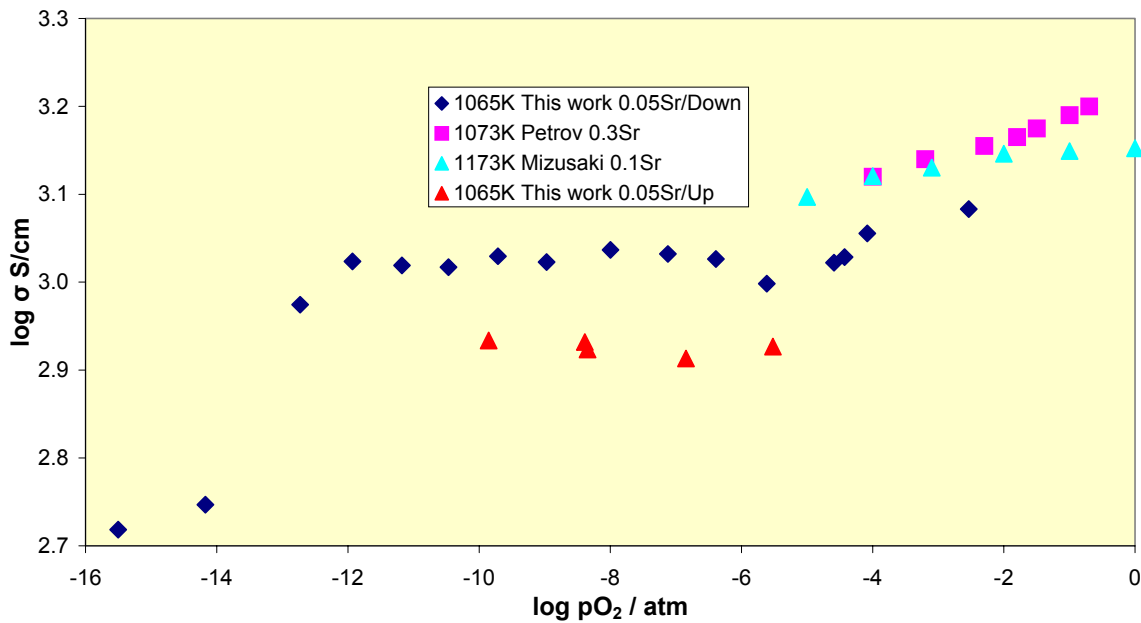


Figure 23: Conductivity of $\text{La}_{0.95}\text{Sr}_{0.05}\text{CoO}_{3-\delta}$ vs. oxygen partial pressure, these results are compared with literature (■, ▲) [71, 72]. The conductivity is measured in stable oxygen partial pressures. At first, the conductivity is measured with going down oxygen partial pressure (down ◇). Next, the oxygen partial pressure is going up and the conductivity is measured again (up ▲).

6.4.2. $(\text{La}_{0.8}\text{Ca}_{0.2})_{1.01}\text{FeO}_{3-\delta}$

The conductivity of $(\text{La}_{0.8}\text{Ca}_{0.2})_{1.01}\text{FeO}_{3-\delta}$ is studied in cell B6S2. The oxygen partial pressure decreased with time in cell B6S2. Thus, the oxygen leakage in this cell remains unknown. Therefore oxygen non-stoichiometry was not able to be determined. We were not able to obtain oxygen partial pressures of lower than $1 \cdot 10^{-6}$ atm by pumping oxygen electrochemical. The cause of this was not able to be determined and will be discussed in chapter 7.

The offset potentials of the new sample holder (S2) with the $(\text{La}_{0.8}\text{Ca}_{0.2})_{1.01}\text{FeO}_{3-\delta}$ sample were measured for many different oxygen partial pressures and at different temperatures to obtain the actual conductivity. These offset potentials vary with oxygen partial pressures and temperatures and are measured for every conductivity measurement.

The conductivity is measured for three different temperatures; 1075, 1125 and 1175 K, see Figure 24. The conductivity decreases with increasing temperature in an oxygen partial pressure range between $1 \cdot 10^{-4}$ to $1 \cdot 10^{-6}$ atm. The equilibration time after a potential step (an oxygen partial pressure step) to obtain stable oxygen partial pressure was obtained after a substantial longer time (2500 min). This equilibration time is much longer than the equilibration times of the AxS1 ($x=0,1,2$) cells. However, the final pump current and thereby the change in oxygen partial pressure is very small. The conductivity was measured two or three times to exclude the influence of unstable oxygen partial pressure. A typical final pump current, oxygen transport through oxygen pump, is in the order of 100 μA and corresponds with 10^{-10} mol O_2/sec .

The activation energy is calculated for three different oxygen partial pressures by plotting the inverse temperature versus the logarithmic-function of the conductivity, see

Figure 24, to obtain an Arrhenius type equation:

$$\sigma = \sigma_0 \times \exp\left(-\frac{Ea}{RT}\right) \quad (47)$$

The slope presents the activation energy divided by the gas constant. The results of the activation energy calculation are outlined in Figure 25.

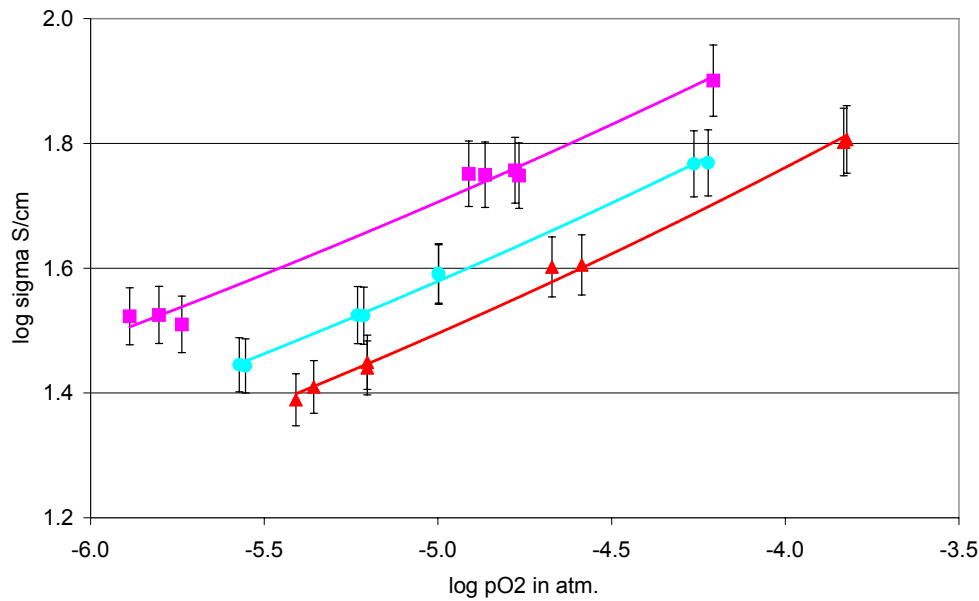


Figure 24: The conductivity of $(\text{La}_{0.8}\text{Ca}_{0.2})_{1.01}\text{FeO}_{3-\delta}$ versus oxygen partial pressure at 1075K (■), 1125K (●) and 1175K (▲).

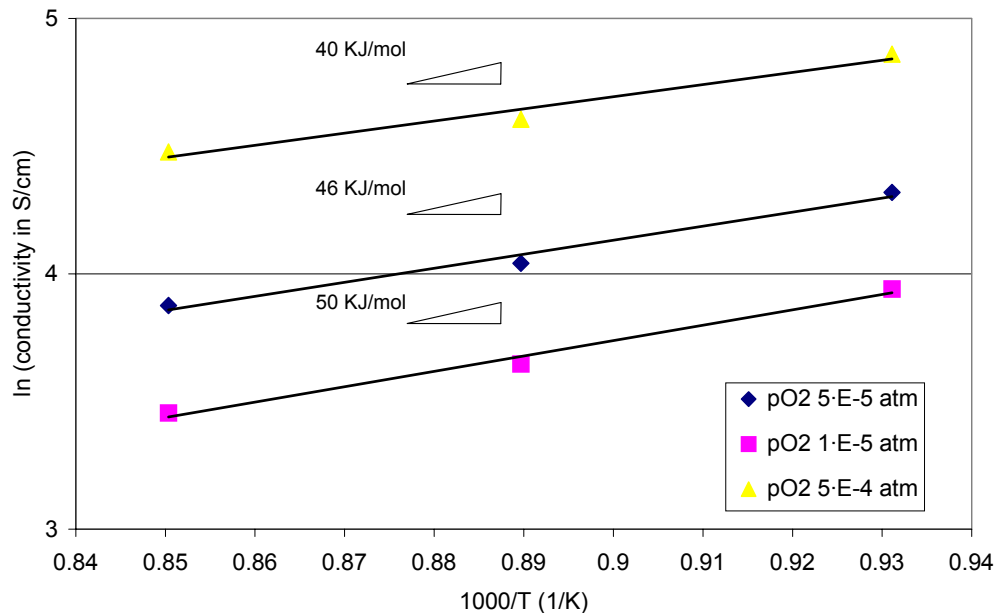


Figure 25: The activation energy of $(\text{La}_{0.8}\text{Ca}_{0.2})_{1.01}\text{FeO}_{3-\delta}$ sample at an oxygen partial pressures of $5 \cdot 10^{-4}$ atm (▲), $1 \cdot 10^{-5}$ atm (◇), and $5 \cdot 10^{-5}$ atm (■).

7. Discussion

7.1. Design

The cell is designed for easy sample and gas change. The disadvantage is the relative large volume. Therefore significant equilibration times (1000 minutes) are obtained. The oxygen leakage was minimised due to the use of grease in the quartz glass joints. Viton O-rings between the YSZ tube and the quartz tube seal the cell gastight. The only detectable oxygen leakage was found in the sealing of the feed-throughs with 'Torr seal'. The location of this an oxygen leakage was found with a helium-test.

The minimal oxygen leakage obtained in this work is $0.4 \mu\text{A}$ ($1 \cdot 10^{-12}$ mol O_2/sec) and is in agreement with literature figures ($0.5 \mu\text{A}/\text{cm}$) [16].

The electrochemical cells, the oxygen sensor and the oxygen pump, exhibit resistance in the order of 2 to 200 Ω indicating good electrical connections. The oxygen sensor and pump (also used as a sensor) showed oxygen partial pressure of $1 \cdot 10^{-5}$ atm for argon, which corresponds with the known amount of oxygen present in this gas.

However, other processes caused an oxygen partial pressures decrease. Therefore, the oxygen leakage was not able to determine. This behaviour was first seen after the conductivity study of $\text{La}_{0.95}\text{Sr}_{0.05}\text{CoO}_{3-\delta}$ sample. The oxygen sensor and the oxygen pump suggest an oxygen partial pressure decrease after flushing with argon (with or without sample in the cell) to an oxygen partial pressure of about $\sim 1 \cdot 10^{-6}$ atm. The possible processes are: The oxygen pump and sensor do not present the actual oxygen partial pressure. Or, and more likely, the cell (sample holder, quartz tube and YSZ tube) obtains oxygen (ab/ad)sorption.

Many materials can cause the oxygen absorption. A black deposit (metallic) is seen on the quartz tube at the cold parts and close to the electrode area on the YSZ tube. This black material is emitted likely from the YSZ tube. The quartz tube is black particularly at the location of the electrodes and less black material is observed at the quartz tube at the height of the spacing between the sensor and pump electrode. The black material is likely to be cobalt or carbon (oxide).

The cobalt originates from the decomposition of the $\text{La}_{0.95}\text{Sr}_{0.05}\text{CoO}_{3-\delta}$ sample. Cobalt (oxide) is known as a reactive material and can diffuse deep into the YSZ tube. Already small amount of cobalt (e.g. 2 at%) colours YSZ blue. This blue colour has not been observed on the YSZ tube. However, a blue spot was observed on the quartz sample holder, close to the location of the sample.

Carbon can originate from the grease. The black material is partly removed by burning locally with flowing air to oxidise the material. Another origin of the carbon is the platinum paste. Platinum paste contains after firing a significant amount of carbon, see Appendix C.

The partial oxygen pressure was monitored after cleaning the quartz tube and the sample holder with nitric acid (65% dilute with 50% Q2 water) and ethanol (A2S1 cell). The black metallic material is partly removed but still visible. The oxygen partial pressure is decreasing similarly as before cleaning, however, the equilibrium is obtained at an oxygen partial pressure of $1 \cdot 10^{-8}$ atm instead of $1 \cdot 10^{-9}$ atm. Thus, the oxygen absorption has been decreased but the problem remains. The cause of the oxygen absorption is so far not conclusive.

The potential of the sensor and pump results in similar results, whereas the pump suggests even lower oxygen partial pressures, which corresponds with higher potential gradient. This

behaviour has been observed after the conductivity study of $\text{La}_{0.95}\text{Sr}_{0.05}\text{CoO}_{3-\delta}$ sample. The higher potential over the oxygen pump than over the oxygen sensor can not be explained by the temperature difference. The oxygen sensor is in the middle of the furnace, whereas the oxygen pump is in the colder part of the furnace. The potential over the oxygen pump is expected to be lower than the potential over the oxygen sensor due to the lower temperature in the same oxygen partial pressure, see equation (1). A possible explanation is the existence of oxygen partial pressure fronts. The oxygen gas diffusion with small concentration gradients can result in long equilibration times and thereby form oxygen partial pressure fronts.

However, the oxygen partial pressure gradient is not likely determined by the small concentration gradients due to the short distance between the electrodes. The equilibration time with a small oxygen partial pressure gradient is in the order of seconds. We found a consequent oxygen partial pressure gradient independent of time.

Ohly [7] found as well in a similar set-up a lower oxygen partial pressure at the oxygen pump than at the oxygen sensor in an oxygen partial pressure range of $1 \cdot 10^{-6}$ to $1 \cdot 10^{-10}$ atm, see appendix A. Ohly [7] suggest that this behaviour is strongly dependent on the gas choice.

The applied potential on the oxygen pump might influence the potential of the oxygen sensor due to the electrical field. Agrawal et al. [33] reported no influence of oxygen pump EMF on the oxygen sensor in case of a distance of 10 mm between sensor and pump. The oxygen pump potential was changed and we found no sudden change at the oxygen sensor within two seconds. The influence of electrical field originated from the oxygen pump is negligible in agreement with [33].

The non-stoichiometry of the samples was not able to determine, due to: At first, the variation of the oxygen leakage in the cell. Second, the disagreement of the amount of oxygen moles pumped in or out the cell and, compared with the increase or decreasing oxygen moles calculated from the oxygen partial pressure obtained at the oxygen sensor.

7.2. Conductivity

The presented conductivity of $\text{La}_{0.95}\text{Sr}_{0.05}\text{CoO}_{3-\delta}$ (Figure 23) is corrected with a fixed offset that is measured in an oxygen partial pressure range of $1 \cdot 10^{-10}$ to $1 \cdot 10^{-14}$ atm. The fixed offset is independent of the oxygen partial pressure in that range and is assumed to be similar in the higher oxygen partial pressure range.

The actual oxygen partial pressures are discussable due to the low amount of oxygen molecules in the cell compared to the amount of oxygen leaked in and electrochemically pumped out. The oxygen leakage and the final oxygen transport through the oxygen pump is in the order of $1 \cdot 10^{-10}$ mol O_2 /sec, whereas the oxygen content in the cell is about $1 \cdot 10^{-3}$ mol O_2 and $\sim 1 \cdot 10^{-10}$ mol O_2 at 1065 K respectively in air and in an oxygen partial pressure of $1 \cdot 10^{-7}$ atm. Despite the relative high oxygen leakage and oxygen transport, the obtained oxygen partial pressure remains stable, e.g. the oxygen partial pressure changed less than 1% in a time scale of 10 minutes. However, the use of a buffer gas such as CO/CO_2 or $\text{H}_2/\text{H}_2\text{O}$ is advisable. Buffer gases are discussed in chapter 9. Oxygen gas diffusion limitations can occur in an oxygen partial pressure lower than $1 \cdot 10^{-7}$ atm and can form oxygen partial pressure fronts. These oxygen partial pressure fronts can be avoided with the use of a buffer gas.

7.2.1. $\text{La}_{0.95}\text{Sr}_{0.05}\text{CoO}_{3-\delta}$

The conductivity of $\text{La}_{0.95}\text{Sr}_{0.05}\text{CoO}_{3-\delta}$ is $1.0 \cdot 10^3$ S/cm at an oxygen partial pressure of $1 \cdot 10^{-5}$ atm at 1065 K and is in agreement with [71, 72]. The results of this work proved that the conductivity is independent of the oxygen partial pressure in the range of $1 \cdot 10^{-6}$ to $1 \cdot 10^{-12}$ atm. In this work, the conductivity decreases significantly by decreasing the oxygen partial pressure below $1 \cdot 10^{-12}$ atm. Increasing the oxygen partial pressure again, the conductivity plateau is found at a lower value. These results suggest a partial decomposition or the formation of a second phase in the $\text{La}_{0.95}\text{Sr}_{0.05}\text{CoO}_{3-\delta}$ material. Small grey spots were observed on the $\text{La}_{0.95}\text{Sr}_{0.05}\text{CoO}_{3-\delta}$ sample under a light microscope.

However, lanthanum cobaltates are known to decompose in an oxygen partial pressure below $1 \cdot 10^{-7}$ atm [9]. The lower oxygen partial pressure, at which the sample decomposes, can be explained by the existence of oxygen partial pressure front. The oxygen partial pressure fronts theory can result in an actual oxygen partial pressure at the oxygen sensor and an other oxygen partial pressure environment near the sample, due to the distance between the sample and oxygen sensor. Note that the conductivity versus oxygen partial pressure of $\text{La}_{0.95}\text{Sr}_{0.05}\text{CoO}_{3-\delta}$ sample is based on only one sample.

7.2.2. $(\text{La}_{0.8}\text{Ca}_{0.2})_{1.01}\text{FeO}_{3-\delta}$

The conductivity of lanthanum ferrates is generally lower than the conductivity of lanthanum cobaltates. However, the lanthanum ferrates are more stable at lower oxygen partial pressure. The conductivity of $(\text{La}_{0.8}\text{Ca}_{0.2})_{1.01}\text{FeO}_{3-\delta}$ decreases with decreasing oxygen partial pressure due to the formation of oxygen vacancies and the reduction of the iron cations from the valence four to three. These processes are enhanced with increasing temperature. This work reveals a conductivity of 38 S/cm for $(\text{La}_{0.8}\text{Ca}_{0.2})_{1.01}\text{FeO}_{3-\delta}$ in an oxygen partial pressure of $1 \cdot 10^{-5}$ atm at 1175 K. The conductivity of $\text{La}_{0.9}\text{Sr}_{0.1}\text{FeO}_{3-\delta}$ in an oxygen partial pressure of $1 \cdot 10^{-5}$ atm at 1175 K is much lower (about 2 S/cm) [75]. The higher conductivity might be explained by the smaller cation size at the B-site. The conductivity $(\text{La}_{0.8}\text{Ca}_{0.2})_{1.01}\text{FeO}_{3-\delta}$ decreases with decreasing oxygen partial pressure as expected from the defectchemistry model describe in chapter 4.

Mizusaki et al. [75] reported an activation energy for the conductivity of 65 and 33 KJ/mol in an oxygen partial pressure of $1 \cdot 10^{-5}$ atm respectively for $\text{La}_{0.9}\text{Sr}_{0.1}\text{FeO}_{3-\delta}$ and $\text{La}_{0.75}\text{Sr}_{0.25}\text{FeO}_{3-\delta}$. The activation energy for the conductivity of $\text{La}_{0.8}\text{Sr}_{0.2}\text{FeO}_{3-\delta}$ will be ~ 45 KJ/mol in similar conditions. An activation energy for the conductivity of 50 KJ/mol was obtained in this work for $(\text{La}_{0.8}\text{Ca}_{0.2})_{1.01}\text{FeO}_{3-\delta}$ under similar conditions. The activation energy for the conductivity decreases with decreasing oxygen partial pressure.

8. Conclusion

8.1. Design

A coulometric titration set-up was designed and the electrical conductivity of mixed-conducting perovskites was studied successfully in a large oxygen partial pressure range at different temperatures. The coulometric titration set-up was designed with easy exchange of samples. The gas system makes it possible to use different kind of gas mixtures to change quickly the atmosphere in the cell. The set-up temperature range is 975 to 1175 K and the lowest obtain oxygen partial pressure is $1 \cdot 10^{-16}$ atm.

The oxygen leakage is about $0.4 \mu\text{A}$ at 1075 K at an oxygen partial pressure of $1 \cdot 10^{-5}$ atm and is in agreement with the literature data of $0.5 \mu\text{A}$ [16]. The oxygen leakage is controlled by the mechanical leakage through the ‘Torr seal’. However, the oxygen partial pressure is not completely under control due to processes that decrease the oxygen partial pressure with time to a constant value.

8.2. Conductivity

The conductivity of $\text{La}_{0.95}\text{Sr}_{0.05}\text{CoO}_{3-\delta}$ is $1.0 \cdot 10^3$ S/cm at an oxygen partial pressure of $1 \cdot 10^{-5}$ atm at 1065 K and in agreement with [71, 72] (see chapter 7.2.1). The conductivity of $\text{La}_{0.95}\text{Sr}_{0.05}\text{CoO}_{3-\delta}$ decreases with the oxygen partial pressure due to the increase of oxygen vacancies and the reduction of the cobalt with a valence of four. The conductivity of $\text{La}_{0.95}\text{Sr}_{0.05}\text{CoO}_{3-\delta}$ at an oxygen partial pressure of $1 \cdot 10^{-5}$ atm at 1065 K suggests an independent of the oxygen partial pressure range of $1 \cdot 10^{-6}$ to $1 \cdot 10^{-12}$ atm at 1065 K. This conductivity plateau can not be explained with the defectchemistry model presented in chapter 4.

$\text{La}_{0.95}\text{Sr}_{0.05}\text{CoO}_{3-\delta}$ decomposes at an oxygen partial pressure lower than $1 \cdot 10^{-12}$ atm at 1065 K. At first, the decomposition is observed by strong decrease of the conductivity with decrease of oxygen partial pressure. The consequence of this decomposition is a lower conductivity plateau after going up in oxygen partial pressure range. Third, the existence of grey spots on the $\text{La}_{0.95}\text{Sr}_{0.05}\text{CoO}_{3-\delta}$ sample can suggest decomposition of the material as well. However, the low decomposition oxygen partial pressure is not in agreement with Bouwmeester et al. [9].

The conductivity of $(\text{La}_{0.8}\text{Ca}_{0.2})_{1.01}\text{FeO}_{3-\delta}$ decreases with decreasing oxygen partial pressure and increasing temperature in the near atmospheric condition. The conductivity of $(\text{La}_{0.8}\text{Ca}_{0.2})_{1.01}\text{FeO}_{3-\delta}$ is 38 S/cm at an oxygen partial pressure of $1 \cdot 10^{-5}$ atm at 1175 K and is much higher than the conductivity of $\text{La}_{0.9}\text{Sr}_{0.1}\text{FeO}_{3-\delta}$ (2 S/cm) [75] in similar conditions. The conductivity activation energy of $(\text{La}_{0.8}\text{Ca}_{0.2})_{1.01}\text{FeO}_{3-\delta}$ is 50 KJ/mol and is in agreement with [75].

9. Recommendations

Design

A coulometric titration set-up with a much smaller reactor volume (in the order of the sample volume) is required to study the non-stoichiometry and oxygen diffusion coefficients. A smaller reactor volume will decrease the oxygen in the gas phase and decrease the equilibration times to obtain stable oxygen partial pressures.

The main challenge of a small volume reactor is that the cell must be sealed gastight at operating temperatures and oxygen partial pressures. A sample is placed in a small bucket and sealed with a plug. There is no sealing method found in the literature that can be used more than once. Thus, the disadvantage of these cells is that for each sample a new coulometric titration cell should be used. An example of a possible coulometric titration cell to study the non-stoichiometry and oxygen diffusion coefficients besides the conductivity is given in appendix C.

The coulometric titration cell in this work proved to have a significant contamination. This contamination is undesired and decreases the oxygen partial pressure in the cell. The contamination can be minimised by; using new and clean quartz tube, sample holder and YSZ tube. The fabrication of the cell must be done with gloves and in a clean environment.

Despite these precautions, contaminations are inevitable. Therefore, the cell must be flushed with a clean gas at (increasing) high temperatures. A clean gas can be argon, technical air should be avoided due to significant contaminations.

The decomposition of samples should be avoided. The samples can release (reactive) metals such as cobalt. These metals deposit on the cold parts of the cell and are able to react with oxygen. The influence of these contaminations on the oxygen partial pressure can be significant. Then oxygen partial pressure can no longer be controlled.

Equilibration times

The equilibration time to obtain stable oxygen partial pressures in the cell is 1000 minutes, typically. The causes of the long equilibration times are the dead gas volume and the thickness of the sample.

The time to obtain oxygen partial pressures equilibration determines the overall speed of the cell to perform oxygen partial pressure steps. The reactor volume in feed-throughs has a significant influence on the equilibration times due to the long oxygen diffusion paths. The amount of the dead volume (and therefore the design of the sample holder and the other parts) is of great importance to the equilibration times. The dead volume of the cell should be minimised in the design of a coulometric titration cell.

Another option to minimise the dead volume is to avoid feed-throughs. External feed-throughs proved to be necessary to avoid decomposition of the 'Torr seal' in the coulometric titration set-up of this work. These feed-throughs increased the dead volume of the cell. Painting platinum wires on the YSZ tube can avoid these feed-throughs. The painted platinum wires are connected with a platinum wire outside the quartz-tube. The platinum paste is painted over the length of YSZ tube. The painted wire must be able to transport electrodes even on the location where the Viton O-rings are situated.

Diffusion limitation occurs in the order of partial pressures of $1 \cdot 10^{-7}$ atm. Therefore, the existence of partial pressure fronts can no longer be neglected. Buffer gases should be used to store and transport these low concentrations. However, the partial pressures of the buffer gases are also controlled with the partial pressure of $1 \cdot 10^{-7}$ atm.

Oxygen absorption

To understand the cause of the oxygen partial pressure decrease observed in cells A2S1 to B6S2 (see Table 5) the following materials should be investigated:

- The black (metallic) material on the quartz tube
- The composition of a new and an used YSZ tube

The composition of the YSZ material must be known to exclude the present of contaminations. Contamination in YSZ can segregate to the surface. These contaminations can be the cause of the observed black material. The composition of the YSZ material is recommended to be studied by an element analysis of the surface with the uses of XPS (X-ray Photoelectron Spectroscopy) and the bulk of the YSZ can be analysed with SEM-EDX (Scanning Electron Microscopy-Energy Dispersive X-ray analysis).

Furnace electric field

The heating coils of the furnace generate an electric field. This electric field influence the obtained potential obtained from the oxygen sensor and oxygen pump. The electric field might also interact with the conductivity measurements on the samples. The influence of this electrical field can be analysed by switching the furnace control unit off and monitoring the potential over the oxygen pump and sensor. The influence of this electrical field on the sample is more difficult to analyse. Ohly [7] suggested a significant influence of the electrical field and therefore applied a grounded shield around the sample holder.

Conductivity

The conductivity results in this work are accurate. However, the offset varies with oxygen partial pressure and temperature and should be measured for each conductivity measurement. The ‘van der Pauw’ technique is used, a power supply applies a potential over two opposite electrodes. This applied potential is between 0.6 and 1V and enables an oxygen vacancy gradient in the mixed-conducting sample. This oxygen vacancy gradient can influence the electronic behaviour of the sample and should be minimised. A lower applied potential for the ‘van der Pauw’ conductivity measurement is recommended.

10. Symbols

$f_{O_2}^{ref}$	oxygen fugacity of the reference
$f_{O_2}^{cell}$	oxygen fugacity in the cell
Pt	Electrodes on the oxygen sensor and pump
F	Faraday constant
R	Gas constant, resistance
T	Temperature
$V_O^{..}$	Oxygen vacancy
O_O^x	Neutral oxygen on a oxygen site
EMF	Potential in volt
I	Current in ampere
Δn_O^{Cell}	Difference in moles of oxygen in the cell
Δn_O^{Sample}	Difference in moles of oxygen in the sample
Δn_O^{Gas}	Difference in moles of oxygen in the gas phase
$n_O^{Leakage}$	Number of oxygen moles that has leaked
α	Constant
e'	Negative charged electron
h^\bullet	Positive charged electron hole
σ_O	Conductivity of oxygen ions
σ_i	Conductivity of ions
σ_e	Conductivity of electrons
t_e	Electron transference number
P_Θ	Oxygen partial pressure where the ionic and electrical conductivity are equal
$V_{Sr}^{..}$	Double negative charged strontium vacancy
$V_{Ti}^{..}$	Negative charged (4) titanium vacancy
V_i	Intrinsic vacancy
$O_i^{..}$	Double negative charged oxygen on an intrinsic site
Y_{Zr}'	Negative charged yttrium on a zirconium site
K_g	Equilibrium constant of gas with the sample
K_{aF}	Equilibrium constant of anti-Frenkel disorder
J_O	Oxygen flux
μ_{O_2}	Oxygen chemical potential
$\mu_{O_2}^0$	Standard oxygen chemical potential
∇c_O	Oxygen concentration gradient
\tilde{D}	Chemical diffusion coefficient
D_0, D_V	Component (vacancy) diffusion coefficient
pO_2	Oxygen partial pressure
c_V	Vacancy concentration
' σ '	Conductivity [S/m] or [1/ Ω m]
' ρ '	Resistivity [Ω m]
'l'	Length of thickness of sample
'd'	Length of thickness of sample



A	Surface area of electrode
V	Volume of the reactor
' $p_{O_2}^f$ '	oxygen partial pressure on equilibrium
' $p_{O_2}^i$ '	Initial measured oxygen partial pressure after potential step
Ea	Activation energy in J/mol
' σ_0 '	Pre exponential factor of the arrhenius type equation

11. Reference

1. Tackett, S.L., *Coulometric titration - new emphasis on an old technique*. Chemtech, 1972: p. 734-740.
2. Szebelledy, L. and Z. Somogyi, *Die Coulometrische Analyse als Präzisionsmethode. I*. Zeitschrift für analytische Chemie, 1938. **112**: p. 313.
3. Wagner, C., *Investigation on silver sulfide*. The journal of chemical physics, 1953. **21**(10): p. 1819-1827.
4. Lankhorst, M.H.R., *Thermodynamic and transport properties of mixed ionic-electronic conducting perovskite-type oxide*. PhD thesis, University of Twente, the Netherlands, 1997.
5. Bakken, E., *Redox energetics and local order in disordered perovskite-type oxide*. PhD thesis, University of Oslo, Norway, 2003.
6. Marques, F.M.B. and G.P. Wirtz, *Oxygen Fugacity Control in Nonflowing Atmospheres .I. Experimental-Observations in CO/CO₂ and O₂/N₂ Mixtures*. Journal of the American Ceramic Society, 1992. **75**(2): p. 369-374.
7. Ohly, C., *Nanocrystalline alkaline earth titanates and their electrical conductivity characteristics under changing oxygen ambients*. Berichte des Forschungszentrums Jülich, 2003. **4070**.
8. Mendybaev, R.A., J.R. Beckett, E. Stolper, and L. Grossman, *Measurement of oxygen fugacities under reducing conditions: Non-Nernstian behavior of Y₂O₃-doped zirconia oxygen sensors*. Geochimica Et Cosmochimica Acta, 1998. **62**(18): p. 3131-3139.
9. Bouwmeester, H.J.M. and A.J. Burggraaf, *Dense ceramic membranes for oxygen separation*, in *The CRC handbook of solid state electrochemistry*, P.J. Gellings and H.J.M. Bouwmeester, Editors. 1997, CRC Press, Boca Raton: Florida, USA. p. 481.
10. Iwase, M., E. Ichise, M. Takeuchi, and T. Yamasaki, *Measurements of the parameter, P_o, for the determinations of mixed ionic and N-type electronic conduction in commercial zirconia electrolytes*. Transactions of the Japan institute of metals, 1984. **25**(1): p. 43-52.
11. Porat, O. and I. Riess, *Double-Solid Electrochemical-Cell for Controlling Oxygen Concentration in Oxides*. Journal of the Electrochemical Society, 1994. **141**(6): p. 1533-1538.
12. Lankhorst, M.H.R. and H.J.M. Bouwmeester, *Determination of oxygen nonstoichiometry and diffusivity in mixed conducting oxides by oxygen coulometric titration .I. Chemical diffusion in La_{0.8}Sr_{0.2}CoO_{3-delta}*. Journal of the Electrochemical Society, 1997. **144**(4): p. 1261-1267.
13. Gellings, P.J. and H.J.M. Bouwmeester, *The CRC handbook of solid state electrochemistry*. CRC Press, Boca Raton, Florida, USA, 1997.
14. Futamata, M., *A Computer-Controlled Measurement System for Electrical- Conductivity Using the Van-Der-Pauw Method at Various Temperatures*. Measurement Science & Technology, 1992. **3**(9): p. 919-921.
15. Boukamp, B.A., *Equivalent circuit, Users manual*. 1989, University of Twente: Enschede, The Netherlands.
16. Belzner, A., T.M. Gur and R.A. Huggins, *Oxygen Chemical Diffusion in Strontium Doped Lanthanum Manganites*. Solid State Ionics, 1992. **57**(3-4): p. 327-337.
17. Gur, T.M., A. Belzner and R.A. Huggins, *A New Class of Oxygen Selective Chemically Driven Nonporous Ceramic Membranes .I. A-Site Doped Perovskites*. Journal of Membrane Science, 1992. **75**(1-2): p. 151-162.
18. Nisancioglu, K. and T.M. Gur, *Potentiostatic Step Technique to Study Ionic Transport in Mixed Conductors*. Solid State Ionics, 1994. **72**: p. 199-203.
19. Figueiredo, F.M., J. Waerenborgh, V.V. Kharton, H. Nafe, and J.R. Frade, *On the relationships between structure, oxygen stoichiometry and ionic conductivity of CaTi_{1-x}Fe_xO_{3-delta} (x=0.05, 0.20, 0.40, 0.60)*. Solid State Ionics, 2003. **156**(3): p. 371-381.
20. Bucher, E., W. Jantscher, A. Benisek, W. Sitte, W. Preis, I. Rom, and F. Hofer, *Transport properties of La_{0.4}Sr_{0.6}CoO_{3-delta}*. Solid State Ionics, 2001. **141**: p. 375-380.

21. Tikhonovich, V.N., E.N. Naumovich, V.V. Kharton, A.A. Yaremchenko, A.V. Kovalevsky, and A.A. Vecher, *Oxygen nonstoichiometry of $Bi_2V_{0.9}Cu_{0.1}O_{5.5-\delta}$ solid electrolyte by coulometric titration technique*. *Electrochimica Acta*, 2002. **47**(24): p. 3957-3964.
22. Tikhonovich, V.N., O.M. Zharkovskaya, E.N. Naumovich, I.A. Bashmakov, V.V. Kharton, and A.A. Vecher, *Oxygen nonstoichiometry of $Sr(Co,Fe)O_{3-\delta}$ -based perovskites I. Coulometric titration of $SrCo_{0.85}Fe_{0.10}Cr_{0.05}O_{3-\delta}$ by the two-electrode technique*. *Solid State Ionics*, 2003. **160**(3-4): p. 259-270.
23. Mizusaki, J., M. Yoshihiro, S. Yamauchi, and F. K., *Nonstoichiometry and defect structure of the perovskite-type oxides $La_{1-x}Sr_xFeO_{3-d}$* . *Journal of Solid State Chemistry*, 1985. **58**: p. 25-266.
24. Mizusaki, J., H. Tagawa, K. Naraya, and T. Sasamoto, *Nonstoichiometry and Thermochemical Stability of the Perovskite-Type $La_{1-x}Sr_xMnO_{3-\sigma}$* . *Solid State Ionics*, 1991. **49**: p. 111-118.
25. Kanai, H., J. Mizusaki, H. Tagawa, S. Hoshiyama, K. Hirano, K. Fujita, M. Tezuka, and T. Hashimoto, *Defect chemistry of $La_{2-x}Sr_xCuO_{4-\delta}$: Oxygen nonstoichiometry and thermodynamic stability*. *Journal of Solid State Chemistry*, 1997. **131**(1): p. 150-159.
26. Ochin, P., C. Petot and G. Petot-Ervas, *Thermodynamic study of point defects in $Cu_{2-d}O$. Electrical conductivity measurements at low oxygen partial pressure*. *Solid State Ionics*, 1984. **12**: p. 135-143.
27. Sockel, H.G. and H. Schmalzried, *Coulometrische titration an Übergangsmetalloxiden*. *Berichte der Bunsengesellschaft*, 1968. **72**(7): p. 745-754.
28. Lade, K. and T. Jacobsen, *Determination of Kinetic and Transport Parameters for Oxygen in Mixed Conductors by an Ac Method*. *Solid State Ionics*, 1994. **72**: p. 218-223.
29. Jacobsen, T., *Energy: proceedings of the second international symposium on solid oxide fuel cells, eds. Grosz F.* 1991: p. p795-800.
30. Tanasescu, S., N.D. Totir and D.I. Marchidan, *Thermodynamic data of the perovskite-type $LaMnO_{3+\delta}$ and $La_{0.7}Sr_{0.3}MnO_{3+\delta}$ by a solid-state electrochemical technique*. *Electrochimica Acta*, 1998. **43**(12-13): p. 1675-1681.
31. Tanasescu, S., N.D. Totir and D.I. Marchidan, *Thermodynamic properties of some perovskite type oxides used as SOFC cathode materials*. *Solid State Ionics*, 1999. **119**(1-4): p. 311-315.
32. Zhang, Q.Z., T. Atake and Y. Saito, *Oxygen Nonstoichiometry in High-Tc Superconductor $Hoba_2Cu_3O_{6+x}$ and Application of Coulometric Tritration*. *Solid State Ionics*, 1992. **50**(3-4): p. 209-216.
33. Agrawal, Y.K., D.W. Short, R. Gruenke, and R.A. Rapp, *The control of oxygen activities in argon-oxygen mixtures by coulometric titration*. *Journal of electrochemical society*, 1974. **121**(3): p. 354-360.
34. Ferreira, A.A.L., J.C.C. Abrantes, J.A. Labrincha, and J.R. Frade, *Oxygen losses and electrical conductivity of $SrTi_{1-y}Nb_yO_{3+\delta}$ materials*. *Journal of the European Ceramic Society*, 1999. **19**(6-7): p. 773-776.
35. Piekarczyk, W., W. Weppner and A. Rabenau, *Dissociation pressure and gibbs energy of formation of $Y_3Fe_5O_{12}$ and $YFeO_3$* . *Material research bulletin*, 1978. **13**: p. 1077-1083.
36. Porat, O. and I. Riess, *Defect Chemistry of $Cu_{2-y}O$ at Elevated-Temperatures .2. Electrical-Conductivity, Thermoelectric-Power and Charged Point-Defects*. *Solid State Ionics*, 1995. **81**(1-2): p. 29-41.
37. Porat, O. and I. Riess, *Defect Chemistry of $Cu_{2-y}O$ at Elevated-Temperatures .1. Nonstoichiometry, Phase Width and Dominant Point-Defects*. *Solid State Ionics*, 1994. **74**(3-4): p. 229-238.
38. Porat, O. and I. Riess, *Partial-Pressure Gradients Due to Temperature-Gradients in a Mixture of Reactive Gases*. *Applied Physics Letters*, 1992. **61**(3): p. 366-368.
39. Porat, O. and H.L. Tuller, *Oxygen nonstoichiometry and defects in Mn-doped $Gd_2Ti_2O_{7+x}$* . *Journal of the American Ceramic Society*, 1996. **79**(12): p. 3078-3082.
40. Riess, I. and O. Porat, *Oxygen partial-pressure measurements under more demanding conditions*. *Solid State Ionics*, 1996. **86-8**: p. 1075-1078.
41. Li, Z.W., Y.D. He and W. Gao, *Use of a solid-state oxygen pump to study oxidation kinetics of Cr and Mo*. *Oxidation of Metals*, 2000. **53**(5-6): p. 577-596.

42. Li, Z.W., Y.D. He and W. Gao, *An ultralow oxygen partial pressure-controlling system and its application to oxidation studies*. Oxidation of Metals, 2000. **54**(1-2): p. 47-62.
43. He, Y., H.Y. Yao, Z.W. Li, H.B. Qi, and F.H. Stott, *A system for measurement of the oxidation kinetics of metals based on solid-state electrochemistry*. Oxidation of Metals, 2000. **53**(3-4): p. 323-339.
44. Gao, W., Z.W. Li, Z. Wu, S. Li, and Y.D. He, *Oxidation behavior of Ni₃Al and FeAl intermetallics under low oxygen partial pressures*. Intermetallics, 2002. **10**(3): p. 263-270.
45. Mitberg, E.B., M.V. Patrakeev, A.A. Lakhtin, I.A. Leonidov, V.L. Kozhevnikov, and K.R. Poeppelmeier, *The relation between high-temperature thermopower, conductivity and oxygen content in YBa₂Cu₃O_{6+x}*. Journal of Alloys and Compounds, 1998. **274**(1-2): p. 103-109.
46. Mitberg, E.B., M.V. Patrakeev, A.A. Lakhtin, I.A. Leonidov, V.L. Kozhevnikov, and K.R. Poeppelmeier, *Intercalation thermodynamics and chemical diffusion of oxygen in the solid solution YBa₂Cu_{3-x}Co_xO_{6+delta}*. Solid State Ionics, 1999. **120**(1-4): p. 239-249.
47. Mitberg, E.B., M.V. Patrakeev, I.A. Leonidov, V.L. Kozhevnikov, and K.R. Poeppelmeier, *High-temperature electrical conductivity and thermopower in nonstoichiometric La_{1-x}Sr_xCoO_{3-delta} (x=0.6)*. Solid State Ionics, 2000. **130**(3-4): p. 325-330.
48. Mitberg, E.B., M.V. Patrakeev, I.A. Leonidov, A.A. Lakhtin, V.L. Kozhevnikov, and K.R. Poeppelmeier, *High-temperature thermodynamics of oxygen equilibrium of solid solutions YBa₂Cu_{3-x}Zn_xO_{6+delta} with gas phase*. Journal of Alloys and Compounds, 1998. **274**(1-2): p. 98-102.
49. Leonidov, I.A., V.L. Kozhevnikov, M.V. Patrakeev, E.B. Mitberg, and K.R. Poeppelmeier, *High-temperature electrical conductivity of Sr_{0.7}La_{0.3}FeO_{3-delta}*. Solid State Ionics, 2001. **144**(3-4): p. 361-369.
50. Kozhevnikov, V.L., I.A. Leonidov, M.V. Patrakeev, E.B. Mitberg, and K.R. Poeppelmeier, *Electrical properties of the ferrite SrFeO_y at high temperatures*. Journal of Solid State Chemistry, 2000. **158**(2): p. 320-326.
51. Kozhevnikov, V.L., I.A. Leonidov, E.B. Mitberg, M.V. Patrakeev, Y.M. Baikov, V.S. Zakhvalinskii, and E. Lahderanta, *High-temperature thermopower and conductivity of La_{1-x}Ba_xMnO₃ (0.02 ≤ x ≤ 0.35)*. Journal of Solid State Chemistry, 2003. **172**(1): p. 1-5.
52. Patrakeev, M.V., I.A. Leonidov, A.A. Lakhtin, E.B. Mitberg, and V.L. Kozhevnikov, *Oxygen nonstoichiometry LaSr₂Fe₃O_{9-x} compounds*. Zhurnal Fizicheskoi Khimii, 1996. **70**(4): p. 611-615.
53. Patrakeev, M.V., I.A. Leonidov, E.B. Mitberg, A.A. Lakhtin, V.G. Vasiliev, V.L. Kozhevnikov, and K.R. Poeppelmeier, *Oxygen thermodynamics and ion conductivity in the solid solution La_{1-x}Sr_xCoO_{3-delta} at large strontium content*. Ionics, 1999. **5**: p. 444-449.
54. Schober, T. and P. Meuffels, *Electrically operated hydrogen and oxygen vacuum leaks using ceramic high-temperature ionic conductors*. Journal of Vacuum Science & Technology a-Vacuum Surfaces and Films, 2001. **19**(3): p. 958-962.
55. Zachau-Christiansen, B., T. Jacobsen and S. Skaarup, *Electrochemical determination of oxygen stoichiometry and entropy in oxides*. Solid State Ionics, 1996. **86-8**: p. 725-731.
56. Ohly, C., S. Hoffmann-Eifert, K. Szot, and R. Waser, *Electrical conductivity and segregation effects of doped SrTiO₃ thin films*. Journal of the European Ceramic Society, 2001. **21**(10-11): p. 1673-1676.
57. Zachau-Christiansen, B., T. Jacobsen, L. Bay, and S. Skaarup, *Surface intermediates on metal electrodes at high temperature*. Solid State Ionics, 1998. **115**: p. 271-277.
58. Zachau-Christiansen, B., T. Jacobsen and S. Skaarup, *Electrochemical determination of oxygen stoichiometry and entropy in oxides*. Solid State Ionics, 1996. **86-8**: p. 725-731.
59. Zachau-Christiansen, B., T. Jacobsen, K. West, and S. Skaarup, *Electrochemical determination of the oxygen stoichiometry in doped ceria*. Solid oxide fuel cells, PV93-4, eds. S.C. Singhal and H. Iwahara (The electrochemical society softbound proceedings series, Pennington, NJ), 1993: p. 104-111.
60. Lankhorst, M.H.R. and H.J.M. Bouwmeester, *Determination of oxygen nonstoichiometry and diffusivity in mixed conducting oxides by oxygen coulometric titration .2. Oxygen nonstoichiometry and defect model for La_{0.8}Sr_{0.2}CoO_{3-delta}*. Journal of the Electrochemical Society, 1997. **144**(4): p. 1268-1273.

61. Lankhorst, M.H.R., H.J.M. Bouwmeester and H. Verweij, *High-temperature coulometric titration of $La_{1-x}Sr_xCoO_{3-\delta}$: Evidence for the effect of electronic band structure on nonstoichiometry behavior*. Journal of Solid State Chemistry, 1997. **133**(2): p. 555-567.
62. Ohly, C., S. Hoffmann-Eifert, K. Szot, and R. Waser, *Defects in alkaline earth titanate thin films - The conduction behavior of doped BST*. Integrated Ferroelectrics, 2001. **38**(1-4): p. 873-881.
63. Ohly, C., S. Hoffmann, K. Szot, and R. Waser, *High temperature conductivity behavior of doped $SrTiO_3$ thin films*. Integrated Ferroelectrics, 2001. **33**(1-4): p. 363-372.
64. Patrakeev, M.V., A.A. Lakhtin, I.A. Leonidov, A.V. Nikolaev, and V.L. Kozhevnikov, *Thermodynamics of $La_3Ba_3Cu_6O_{14+x}$ Oxidation*. Zhurnal Fizicheskoi Khimii, 1995. **69**(3): p. 403-407.
65. Patrakeev, M.V., I.A. Leonidov, A.A. Lakhtin, and V.L. Kozhevnikov, *Thermodynamics of interaction between $(Nd_{2/3}Ce_{1/3})_4(Ba_{2/3}Nd_{1/3})_4Cu_6O_{16+x}$ and oxygen in the gas phase*. Zhurnal Fizicheskoi Khimii, 1995. **69**(11): p. 1952-1955.
66. Patrakeev, M.V., I.A. Leonidov, A.A. Lakhtin, V.L. Kozhevnikov, and A.V. Nikolaev, *Oxygen Nonstoichiometry in $PrBa_2Cu_3O_{6+x}$ Compound*. Zhurnal Fizicheskoi Khimii, 1994. **68**(12): p. 2239-2243.
67. Patrakeev, M.V., E.B. Mitberg, A.A. Lakhtin, I.A. Leonidov, V.L. Kozhevnikov, and V.I. Voronin, *High-temperature equilibrium between $YBa_2Cu_{3-x}Co_xO_{6+\delta}$ solid solutions and oxygen*. Inorganic Materials, 2000. **36**(5): p. 474-478.
68. Waernhus, I., *Defect chemistry, conductivity and mass transport properties of $La_{1-x}Sr_xFeO_{3-\delta}$ ($x=0$ and 0.1)*, in *Institute of material technology*. 2003, NTNU, Norway: Trondheim.
69. Vanhassel, B.A., T. Kawada, N. Sakai, H. Yokokawa, M. Dokiya, and H.J.M. Bouwmeester, *Oxygen Permeation Modeling of Perovskites*. Solid State Ionics, 1993. **66**(3-4): p. 295-305.
70. Mizusaki, J., Y. Mima, S. Yamauchi, K. Fueki, and H. Tagawa, *Nonstoichiometry of the Perovskite-Type Oxides $La_{1-x}Sr_xCoO_{3-\delta}$* . Journal of Solid State Chemistry, 1989. **80**(1): p. 102-111.
71. Petrov, A.N., O.F. Kononchuk, A.V. Andreev, V.A. Cherepanov, and P. Kofstad, *Crystal-Structure, Electrical and Magnetic-Properties of $La_{1-x}Sr_xCoO_{3-y}$* . Solid State Ionics, 1995. **80**(3-4): p. 189-199.
72. Mizusaki, J., J. Tabuchi, T. Matsuura, S. Yamauchi, and K. Fueki, *Electrical-Conductivity and Seebeck Coefficient of Nonstoichiometric $La_{1-x}Sr_xCoO_{3-\Delta}$* . Journal of the Electrochemical Society, 1989. **136**(7): p. 2082-2088.
73. Dyer, *Mixed conducting membranes for syngas production*, in *United states patent*. 2002, Air products and chemicals, Inc.,: U.S.A.
74. van Doorn, R.H.E., H. Kruidhof, A. Nijmeijer, L. Winnubst, and A.J. Burggraaf, *Preparation of $La_{0.3}Sr_{0.7}CoO_{3-\delta}$ perovskite by thermal decomposition of metal-EDTA complexes*. J. Mater. Chem., 1998. **8**: p. 2108-2112.
75. Mizusaki, J., T. Sasamoto, W.R. Cannon, and H.K. Bowen, *Electrical-Conductivity and Seebeck Coefficient, and defect structure of $La_{1-x}Sr_xFeO_3$ ($x=0.1, 0.25$)*. Journal of the American Ceramic Society, 1983. **66**(4): p. 247-252.
76. Tanasescu, S., D. Berger, D. Neiner, and N.D. Totir, *Thermodynamic characterisation of some doped lanthanum chromites used as interconnects in SOFC*. Solid State Ionics, 2003. **157**(1-4): p. 365-370.

12. Dankwoord

De aanbeveling van de lagere school was om MAVO of HAVO te gaan doen. De middelbare school stelde dat ik het beste HAVO kon gaan doen. Na het VWO heb ik gekozen om een technische universitaire studie te gaan doen. Zeven jaar later ben ik beland bij het einde van mijn studie chemische technologie. Hier ben ik trots op, maar dat had ik niet kunnen doen zonder de mensen en vrienden om mijn heen. Ik ben jullie dan ook heel erg dankbaar voor.

Ten eerste wil de mensen bedanken die mij hebben geholpen bij het afstuderen. Ik begin met de commissie. Frederic, een leukere begeleider had ik niet kunnen krijgen. Je wilde altijd tijd voor me vrijmaken, en je wilde zelfs metingen voor mij doen. Sorry dat ik je voetbal en volleybal team moet verlaten. Je bent zelfs zo fanatiek dat je me versloeg met “Smack the Pingu”. “Bernard heb je even?” Bernard: “George, voor jou altijd.” Volgens mij is er een periode geweest dat ik elke dag bij je langskwam met vragen, omdat ik geen uitweg meer zag. En telkens had je weer een briljant idee die ons project weer verder bracht. Henny....je hebt het altijd druk. Maar je deur stond altijd open. Als ik met je sprak over materiaalkunde, bleek je het helemaal niet meer druk te hebben. Geweldig! Maar waar ik je het meest dankbaar voor ben, is de promotie plaats die je voor mij geregeld heb. Dave wil ik ook graag bedanken voor de tijd die je voor mij nam. Nikolaos Bonanos, it is an honour that you were willing to join my graduation-committee. I am very pleased that you even want to visit us and to travel all over from Denmark.

Maar ik zou ook graag de hele vakgroep willen bedanken. Met name; Louis voor de interessante vakken die je hebt gegeven. Maar ook Attila, ik heb je (te) veel gevraagd. Ook Ruud wil ik bedanken voor het maken van maar liefst zes cellen en aanpassingen. Daarnaast had ik nooit de opstelling in elkaar kunnen zetten met behulp van en de technische kennis van Gerrit. Het studentenhok was eigenlijk te gezellig. Arjen, Alisia, Sjoerd, Ard, Paul, Gerwin, Itxaro, Stijn en Maarten het was heerlijk.

Ik heb veel te danken aan mijn vriendin Jitka, zonder haar had ik de studie nooit zo snel afgemaakt. Imelda bedankt voor de stimulans. Mijn ouders Bert en Christien, broer Herbert, zus Marisa en Simone, erg bedankt dat jullie mij altijd zijn blijven steunen. Ik wil ook mijn studie (jaar) genoten bedanken die er voor gezorgd hebben dat ik te lang over mijn P heb gedaan. Te veel lol met jullie. Die leuke tijd heb ik ook met Herrie, vele Alohanen en vrienden (o.a. autoclub Rob, Robbie en Bert) meegemaakt. Daarnaast is mijn muziekbond met o.a. Ferry een gave aanvulling geweest op mijn studie.

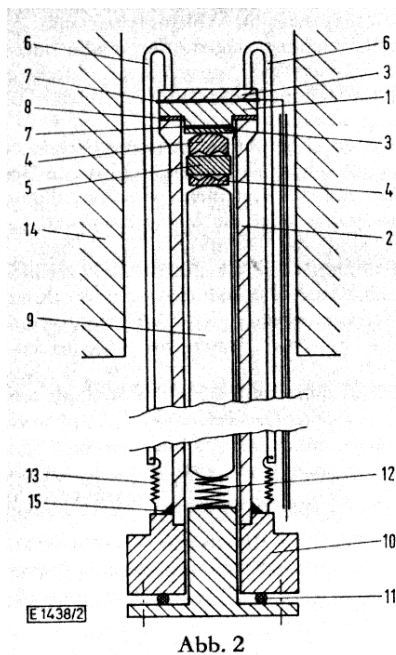
Sorry voor degene die ik niet bedankt heb.

Kortom, allemaal bedankt. Het studeren was zo leuk, dat ik me nog verder ga ontwikkelen.

Appendix A – Coulometric titration set-ups

Socket et al.

Socket et al. [27] designed in 1968 a coulometric titration set-up to study the non stoichiometry of nickel oxide, cobaltate, ferrite, and cobalt doped ferrite. They obtained an oxygen partial pressure of 10^{-12} atm at 1473 K with a CSZ electrolyte, see Figure 26. The sample (5) is located between two alumina rods (4). The electrolyte (1) is covered with two electrodes (7) and placed on top of the sample. An alumina disc (3) is positioned above the electrolyte. The sample is placed in a quartz tube (2). The dead volume is reduced with a closed quartz tube (9). The electrode and alumina rod are pressed together by two springs (12, 13). The electrolyte is sealed on the quartz tube by using ‘Solidex glass pulver’(8). The quartz tube is gas tight sealed (11, 15) on a metal block (10). The time to obtain stable ‘EMF’ was varied between 15 minutes and several hours after changing the current. This time is dependent on temperature. The maximum applied potential is 1 V. The obtained oxygen leak is $1 \cdot 10^{-6}$ g O_2/h , which corresponds with a specific oxygen leak of about 10 mA/cm^2 (electrode area of 3 cm^2).



$V_{\text{cell}} \approx 7-10 \text{ cm}^3$
 $M_{\text{sample}} \approx 5 \text{ g (estimated)}$
 Specific oxygen leakage $\approx 10 \text{ mA/cm}^2$
 Carrier gas = H_2
 Current = 3-8 mA

Figure 26, CT-design by Socket et al. [27]

Piekarczyk et al.

Piekarczyk et al. [35] studied the thermodynamic properties yttrium ferrites in 1978 with the use of an electrochemical solid state cell. The materials were characterised over a temperature range of 1173-1523 K, the lowest oxygen partial pressure measured was 10^{-12} atm. ($T=1173$ K). The electrochemical cell contained a platinum oxide-electrode in air, calcium doped zirconia as electrolyte on top of the sample acting as the second electrode. Two undesired influences were observed at temperature higher than 1273 K: Oxygen permeation through the electrolyte and reactions between sample and electrolyte. The problems were solved by placing the sample in an alumina crucible inside a zirconia tube, which is placed in another zirconia tube, see Figure 27. The sealed zirconia tubes forming four electrochemical cells pair

wise in series. The smallest tube (A) has no direct contact with air. The oxygen partial pressure between the tubes A and B is maintained at the same oxygen partial pressure as inside tube A to avoid oxygen permeation and is controlled by electrochemical oxygen pump. The galvanic cells were degassed at about 573 K and then filled with pure argon. The temperature was raised and the oxygen partial pressure inside tube A was obtained by measuring the EMF over the reference electrode (air) and electrode inside tube A. An accuracy of 1 mV was obtained by the use of a Keithley 616 digital electrometer. The time to reach equilibrium varied from a few to several tens of hours.

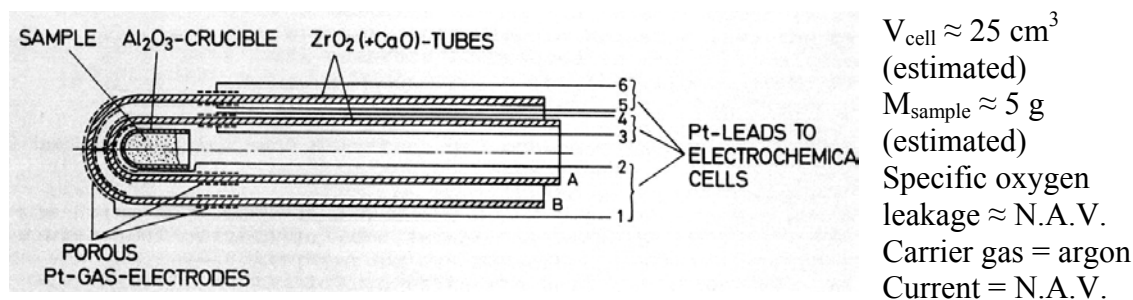


Figure 27 Coulometric titration set-up designed by Piekarczyk et al. [35]

The most important challenge in coulometric titration is the oxygen leakage. The oxygen leakage can be minimised by lowering the oxygen partial pressure gradient over the electrolyte material as discussed in paragraph ‘Oxygen leakage’ [11].

Porat, Riess and co-workers

The coulometric titration double-cell design of Porat and Riess [11] is an extension of the design presented by Piekarczyk et al. [35]. Porat and Riess used two similar electrolyte tubes placed parallel inside a quartz tube instead of a smaller tube enclosed in a bigger tube. One electrolyte tube is placed in a quartz tube with the sample. The part of the quartz tube with the sample is placed in furnace 2. Furnace 1 is maintained at an ideal temperature for ionic conductivity of the electrolyte (calcium doped zirconia). Furnace 2 can control the temperature of the sample.

The sample and an electrolyte tube are placed in a sealed quartz tube. This quartz tube and the second electrolyte tube are placed in a larger quartz tube and sealed with a brass fitting, see Figure 28, Figure 29, Figure 30. The air inside the inner cell replaced by 0.3 atm argon, which is purified from oxygen by titanium sponge at 1000 K. The gas volume of the inner tube (dead volume) is 50 cm³.

Temperature gradient between sample and oxygen sensor can be a problem when reactive gases (CO or H₂) are used. Oxygen pressure gradients can be formed due to the reaction constant on temperature. Oxygen pressure gradients due to thermal diffusion can be neglected [38]. Water vapour is hard to avoid and is in equilibrium with hydrogen and oxygen. Therefore, water vapour is the most commonly reactive gas, originates from wet atmosphere and degassing. As the partial pressure of water in an extremely dry atmosphere is at least 10⁻⁸ atm, it is obvious that experiments may be affected by the presence of water.

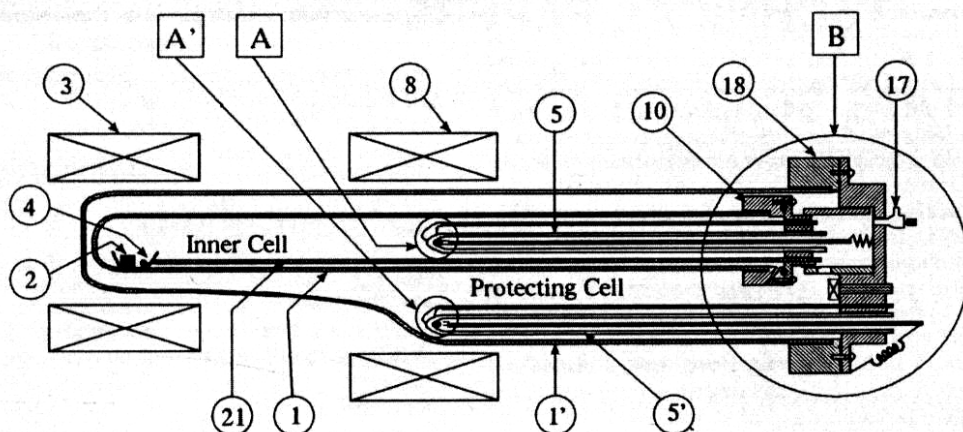


Figure 28 Coulometric titration set-up by Porat and Riess, overview [11]

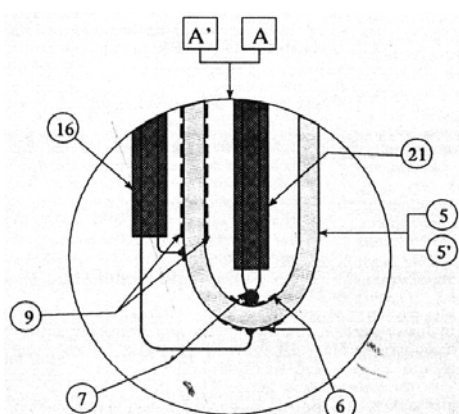


Figure 29 CT (Porat and Riess), electrolyte tip [11]

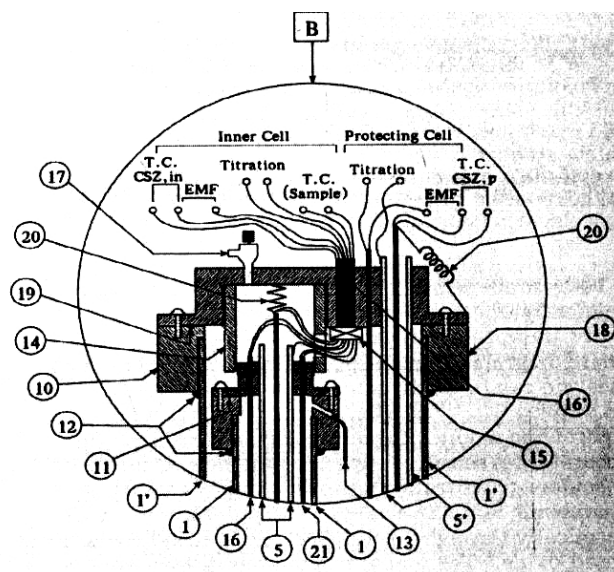


Figure 30 CT (Porat and Riess), fitting brass [11]

The conductivity of Cu_{2-y}O bars are studied in an oxygen partial pressure range of $10^{-12} - 0.15$ atm at temperatures between 900 – 1300 K [36]. At low temperature, the conductivity of Cu_{2-y}O could not be measured in their CT cell due to the long time required for equilibration with the surrounding atmosphere. They performed preliminary measurements to determine the amount of oxygen in the cell is reported in [37].

The oxygen partial pressure is measured with an alumina dummy sample to exclude the oxygen exchange with the sample. A linear relation between $p\text{O}_2$ and $n\text{O}_2$ is observed at constant sample temperature. The cell is pumped to 1 Pa (10^{-5} bar) at 400 K and then filled with pure dried ($P_{\text{H}_2\text{O}} < 3 \cdot 10^{-8}$ atm) argon (99.99%) to 0.3 atm. This step is repeated 3-4 times.

The water partial pressure is hard to avoid, water originates from the wet atmosphere and from degassing. Argon is wetted deliberately in oxygen partial pressure lower than 10^{-8} atm. The water partial pressure acts as a buffer gas.

Oxygen titration to oxidise Cu to Cu_{2-y}O takes a few days. The oxygen partial pressure is determined from the EMF after relaxation. The relaxation time can vary from few minutes (high temperature) to nearly a day (low temperature or low oxygen partial pressure).

The non-stoichiometry of manganese doped gadolinium titanates is studied by Porat et al. [39] In this study, the same set-up is used. However, the total pressure (argon) is installed slightly above 1 atm overpressure to reduce the gas (e.g. oxygen) leakage.

$$V_{\text{cell}} \approx 50 \text{ cm}^3$$

$$M_{\text{sample}} = 0.3 \text{ g powder and } 0.5 \text{ g bar}$$

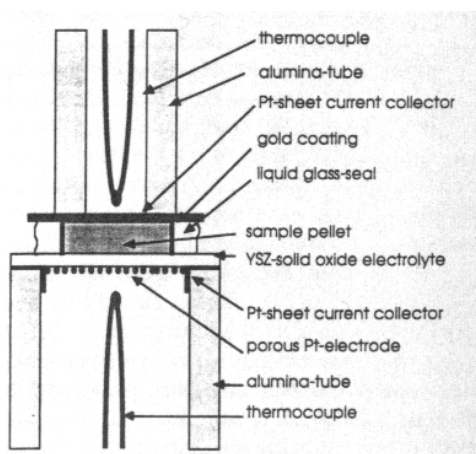
No leakage obtained between 10^{-4} and 10^{-12} atm

Carrier gas = Ar, CO₂ and H₂

$$\text{Current} = 100 \mu\text{A} - 10 \text{ mA}$$

Gür and Belzner and co-workers

Gür and Belzner and co-workers [16-18] measured the chemical diffusion in strontium doped lanthanum manganites and iron doped strontium cobaltates in a temperature range of 950 – 1300 K. The oxygen partial pressure was controlled between 10^{-9} to 0.21 atm, see Figure 31. The samples were placed on a polished YSZ disc, one polished side was coated with platinum to act as a reference electrode. The samples are coated with gold to act as an electrode. The non-porous gold layer prevented the sample from reacting with the glass seal and also acted as an additional diffusion barrier for oxygen. The ring space remaining around the sample was filled with Pyrex powder in order to minimise the dead volume. The maximum applied potential is 20 mV to avoid segregation of oxygen bubbles in the sample and in the electrolyte. The electrolyte has a diameter of 12 mm, the electrode area is around 0.2 cm².



$$V_{\text{cell}} \approx V_{\text{sample}}$$

$$M_{\text{sample}} \approx 0.1 \text{ g}$$

$$\text{Specific oxygen leakage} \approx 0.1 \mu\text{A}/\text{cm}^2$$

Carrier gas = no gas present

$$\text{Current} = 100 \mu\text{A}$$

Figure 31, CT-design by Belzner et al. [16]

Lankhorst

Lankhorst [4] placed a sample in an alumina bucket and sealed the bucket with an electrolyte (YSZ) disc. The electrolyte is covered with three platinum oxide electrodes acting as oxygen pump and sensor, see Figure 33. This design is similar to the one used by Gür and Belzner [16, 17]. However, this design showed significant polarization losses at the electrode in reducing environment. Lankhorst [4] improved the design, which is based on the work of Lade and Jacobsen [28], see Figure 32. In this design, a YSZ bucket replaces the alumina bucket. The YSZ bucket functions as a second electrochemical cell. The coulometric titration cell is placed in a quartz tube flushed with air as reference oxygen fugacity. The oxygen partial pressure domain is between 10^{-4} and 1 atm in a temperature range of 973-1273 K, these conditions were chosen to study the chemical diffusion and the non-stoichiometry of oxygen in strontium doped lanthanum cobaltates and strontium doped lanthanum ferrites. However, the oxygen partial pressure and temperature domain of this set-up is much larger.

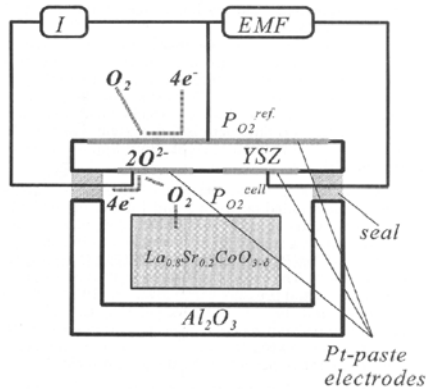


Figure 32, CT set-up designed by Lankhorst 1

$$V_{\text{cell}} \approx 0.25 \text{ cm}^3$$

$$M_{\text{sample}} \approx 0.2 \text{ g}$$

Specific oxygen leakage \approx N.A.V.

Carrier gas = hardly any gas present

Current = N.A.V.

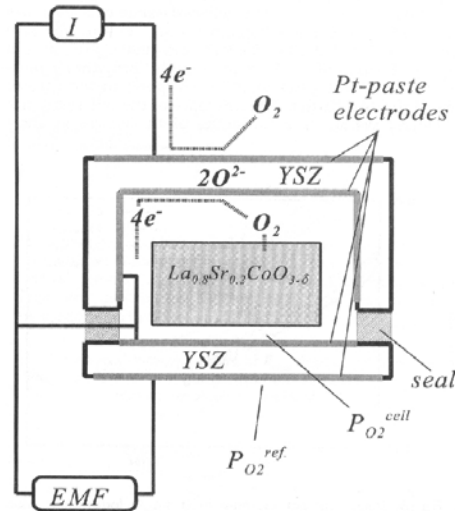


Figure 33, CT set-up designed by Lankhorst 2

Lade and Jacobsen

Lade and Jacobsen [28, 29] used CT as a method to determine the chemical diffusion coefficient and surface kinetics of oxygen in mixed conducting oxides (strontium doped lanthanum manganites). The oxygen partial pressure can be controlled between $8 \cdot 10^{-5}$ and 0.2 atm, corresponding to 0 to 200 mV potential difference over the electrolyte (YSZ), in a temperature range of 1173-1273 K, see Figure 34. The sample is placed in an alumina bucket covered with an YSZ disc sealed with a golden ring.

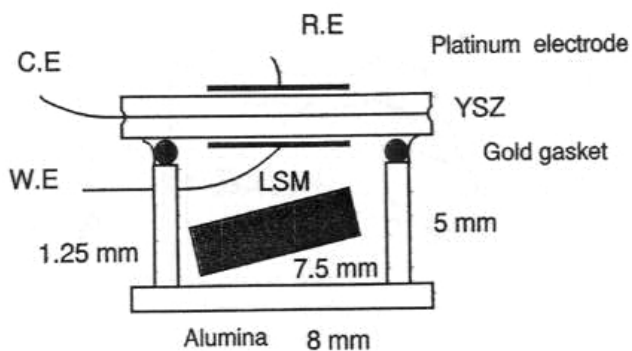


Figure 34, CT design by Lade et al. [28, 29]

$$V_{\text{cell}} \approx 0.15 \text{ cm}^3$$

$$M_{\text{sample}} \approx 0.7 \text{ g}$$

Specific oxygen leakage \approx N.A.V.

Carrier gas = hardly any gas present

Current = N.A.V.

Zachau-Christiansen et al. [57-59] continued the work of Lade et al. [28] and changed the cell by replacing the third (counter) electrode, see Figure 35. They measured the non-stoichiometry of gadolinium doped ceria and calcium doped ceria powder in a oxygen partial pressure range of 10^{-20} to 0.21 atm in a temperature domain of 1073-1273 K. A stable EMF was obtained after 13 hours after a potential step at 1273 K. The resistance over the electrochemical cell is 5Ω at 1273 K.

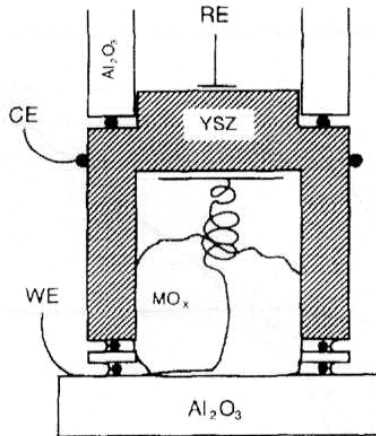
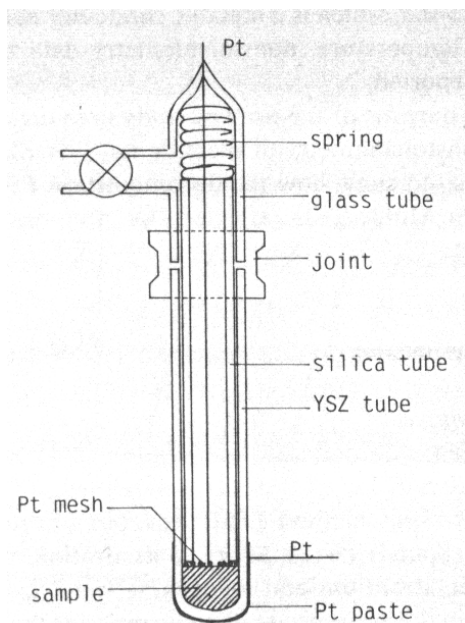


Figure 35, CT design of Zachau-Christiansen et al. [58, 59]

Mizusaki et al.

Mizusaki et al. [23-25] studied the non-stoichiometry strontium doped lanthanum ferrite, strontium doped lanthanum manganite and, strontium doped lanthanum copper oxide powder by thermogravimetry and coulometric titration. The environment was controlled in a temperature range of 673 to 1273 K and in a oxygen partial pressure between 10^{-3} to 10^{-20} atm. The powder is directly connected to the electrolyte. A disadvantage of this set-up is that the powder might interact with the electrolyte, see Figure 36.



$V_{\text{cell}} \approx 25 \text{ cm}^3$
 $M_{\text{sample}} \approx 0.7 \text{ g}$
 Specific oxygen leakage $\approx \text{N.A.V.}$
 Carrier gas = argon
 Current = $50 \mu\text{A} - 2\text{mA}$

Figure 36, CT design by Mizusaki et al. [23-25]

Tikhonovich et al.

Tikhonovich et al. [21, 22] studied the oxygen deficiency of $\text{Bi}_2\text{V}_{0.9}\text{Cu}_{0.1}\text{O}_{5.5-\delta}$ and the oxygen non-stoichiometry of chromium and iron doped strontium cobaltates in a oxygen

partial pressure range of $8 \cdot 10^{-10}$ to 0.21 atm by using the coulometric titration technique in a temperature range of 650-1250 K. The cell A, Figure 37, designed by Tikhonovich, is based on the coulometric titration cell design of Lankhorst [4]. The sample (1) is placed in a YSZ bucket and covered with a YSZ top (2). The YSZ materials are sealed with glass-ceramic sealant (5). The electrodes (3) and the wires (4) are made of platinum. The temperature is measured with thermocouple (6). Cell B is designed to measure the oxygen deficiency in non-isothermal condition. The oxygen partial pressure relaxation takes 3 to 40 hours and is caused by the equilibriums in porous platinum oxide.

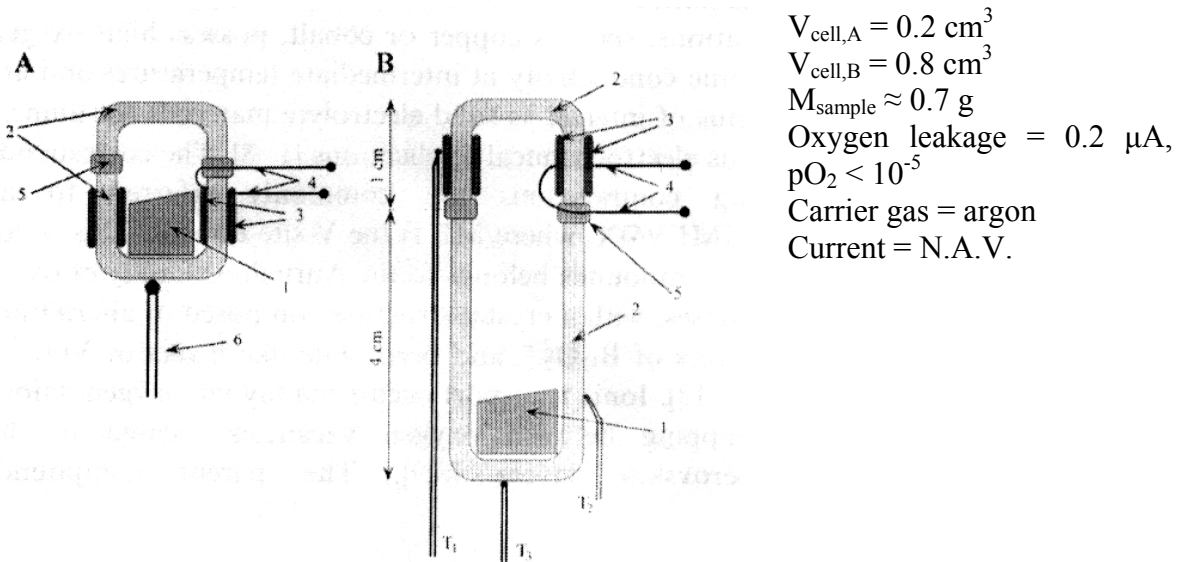
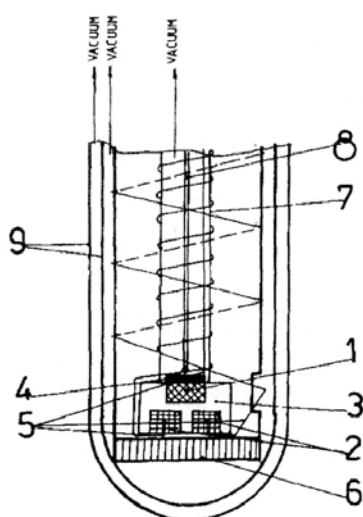


Figure 37, A and B CT designs of Tikhonovich [21, 22]

Tanesescu et al.

Tanesescu et al. [30, 31, 76] studied the thermodynamic data of perovskite materials based on strontium doped lanthanum manganite and doped lanthanum chromites by coulometric titration over a temperature range of 1073-1373 K. They used a three electrode galvanic cell, of which two iron-wüstite electrodes are used to titrate oxygen and the other as reference, to record the EMF (sensor). The sample is the third electrode. The cell, see Figure 38, is rinsed with argon and sequenced by vacuum pumping to 10^{-9} atm. The temperature is increased after the evacuation. The sample (1) is placed on YSZ electrolyte (3) which is connected with two iron wüstite electrodes (2). The sample is covered with platinum plate (4), the wires (5) are made of platinum. The electrodes are positioned on a quartz plate (6) held by a quartz tube (7). The tube is placed in another quartz tube (9) with a thermocouple (8). The oxygen partial pressure can be lowered to 10^{-18} atm. by electrochemical pumping using a Tacussel potentiostat (Bi-PAD) with a constant current of 80 μ A with a maximal overvoltage 30 mV. The EMF (of the sensor) is measured after equilibrium of the sample and took typically 3 to 4 hours. The EMF measurements are recorded with a digital multimeter “Keithley 197A”.

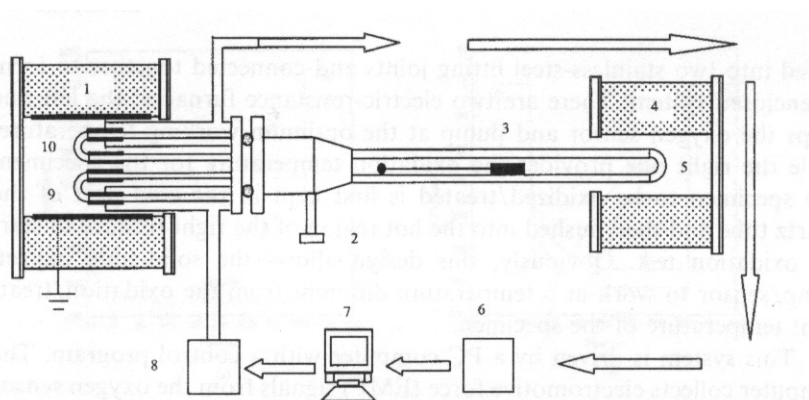


$V_{\text{cell}} \approx 0.5 \text{ cm}^3$
 $M_{\text{sample}} = 0.04 \text{ g}$
 Oxygen leakage \approx N.A.V.
 Carrier gas = argon
 Current = $80 \mu\text{A}$

Figure 38, CT design by Tanasescu et al. [30, 31]

Li et al.

Li et al. [41-44] developed a coulometric titration set-up to study the oxidation of Ni-Cr alloy, chrome, molybdenum, iron, zirconium, titanium, nickel and copper. They used a set-up with two furnaces, one (1) for achieving an optimum working environment for YSZ electrolytes as oxygen pump (9) and sensor (10) and second furnace (4) for changing the temperature of the sample, see Figure 39. The sample (3) is placed in a quartz tube (5), which is attached to the electrolytes by a connector (2). The sensor and pump are monitored and controlled by a computer (6, 7, 8). They report a stable environment in a oxygen partial pressure range of 10^{-23} at 973 K. The lower oxygen partial pressure limit mainly depends on the leakage of the system and the electrochemical semi-permeability of the solid-state electrolyte. The composition and the microstructure of the electrolyte material and its working temperature have important influences on the electronic conductivity of the electrolytes. It took 24 hours to reach an oxygen partial pressure of 10^{-23} atm at 1073 K and only 2 hours at 973 K. The oxygen transport, especially in low oxygen partial pressure, is relatively slow in this design due to the separation of the electrolytes and sample into two furnace.

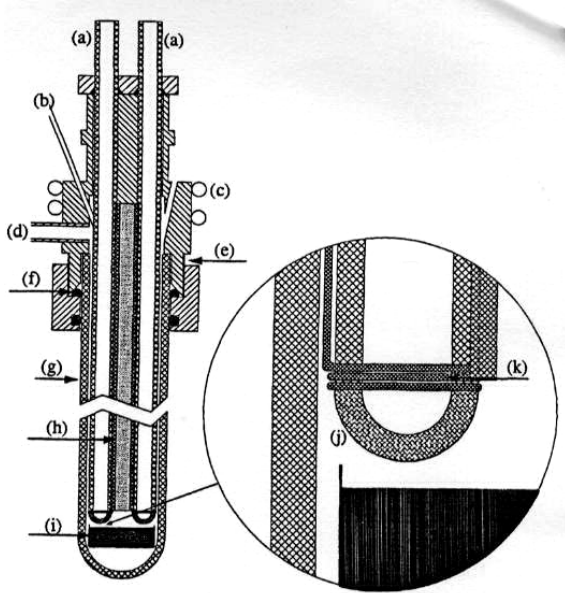


$V_{\text{cell}} \approx 40 \text{ cm}^3$
 $M_{\text{sample}} = 0.3 \text{ g}$
 Oxygen leakage \approx N.A.V.
 Carrier gas = argon
 Current = N.A.V.

Figure 39, CT Design of Li, He and Gao [41-44]

Bakken

Bakken [5] studied the non-stoichiometry of strontium ferrite and calcium manganite at 1223 – 1373 K in a oxygen partial pressure range of 10^{-12} to 0.21 atm by using coulometric titration, see Figure 40.



$$V_{\text{cell}} \approx \text{N.A.V}$$

$$M_{\text{sample}} = \text{N.A.V}$$

$$\text{Specific oxygen leakage} \approx 400 \mu\text{A}/\text{cm}^2$$

Carrier gas = argon

$$\text{Current} = \text{N.A.V.}$$

Figure 40, CT design by Bakken et al. [5]

Ferreira et al.

Ferreira et al. [34] obtained a oxygen partial pressure of 10^{-16} atm at 1273 K. They studied the oxygen losses and electrical conductivity of niobium doped strontium titanates by a CT set-up derived from Lankhorst [4].

$$V_{\text{cell}} \approx 0.25 \text{ cm}^3$$

$$M_{\text{sample}} \approx 0.2 \text{ g}$$

Specific oxygen leakage \approx N.A.V.

Carrier gas = hardly any gas present

$$\text{Current} = \text{N.A.V.}$$

Figueiredo et al.

Figueiredo et al. [19] studied the ionic conductivity of iron doped calcium titanate in an oxygen partial pressure environment of 10^{-5} to 0.21 atm with a commercial available oxygen sensor (Oxylyt, Sensotech Magdeburg, Germany) as coulometric titration set-up. Argon was transported through an oxygen sensor (cell #1) followed through a sample furnace and sequenced by a second oxygen sensor (cell #2), see Figure 41. The difference in oxygen partial pressure between the sensors was adsorbed or de-adsorbed by the sample. Bucher et al. [20] used the same oxygen sensor to measure the electronic conductivity and chemical diffusion of lanthanum strontium cobaltate in a oxygen partial pressure range down to 10^{-4} atm at 923-1173 K.

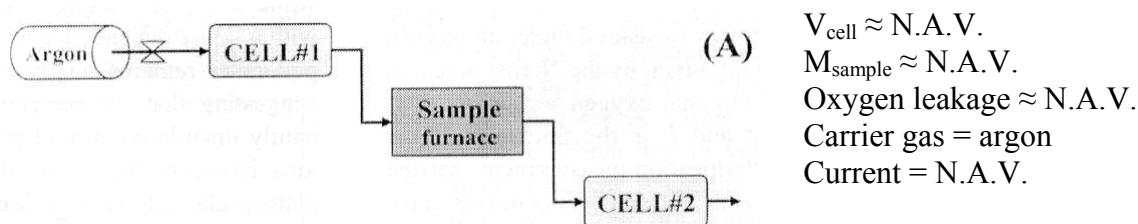
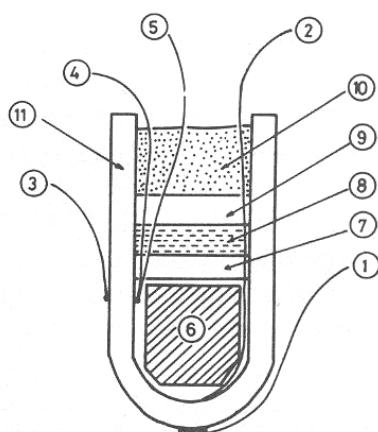


Figure 41, Schematic set-up by Figueiredo et al. [19]

Zhang et al.

Zhang et al. [32] studied the electrical conductivity and non-stoichiometry of high- T_c superconductor $\text{HoBa}_2\text{Cu}_3\text{O}_{6+x}$ in a oxygen partial pressure range of $5 \cdot 10^{-6}$ to 0.21 atm at temperatures of 863-1173 K. The electrical conductivity was measured with the ‘Van der Pauw technique’. A stable EMF is obtain after 2 hours at 1173 K. The sample in a bar shape is placed in a YSZ crucible. The dead volume is decreased by filling the YSZ crucible with high purity alumina pieces. The non-stoichiometry of $\text{HoBa}_2\text{Cu}_3\text{O}_{6+x}$ powder (6) wrapped in a gold foil was placed in a YSZ crucible (11). The oxygen content is measured with electrodes (1 and 2) and controlled with electrode (3 and 4). The sample is covered with an alumina disk (7) and attached with the YSZ crucible using alumina cement (8). The YSZ tube was further sealed with glassy material (9 and 10).



$V_{\text{cell}} \approx V_{\text{sample}}$
 $M_{\text{sample}} \approx 0.6 \text{ g}$
 Oxygen leakage $\approx \text{N.A.V.}$
 Carrier gas = hardly any gas present
 Current = 10-30 μA

Figure 42, Coulometric titration set-up of Zhang et al. [32]

Ohly et al.

Ohly et al. [7, 56, 62, 63] investigated the electrical conductivity of (barium doped) strontium titanates at 973 – 1273 K. The oxygen atmosphere was controlled by a coulometric titration and varied between 10^{-20} and 0.21 atm. The sample is connected by 4 wires for electrical conductivity measurement with ‘Van der Pauw’ technique, see Figure 44. An alumina tube positions the sample, which is located in a long YSZ tube acting as oxygen sensor at the tip (close to the sample) and as oxygen pump, see Figure 43. The electrodes of the oxygen pump are 130 mm long. The YSZ tube is placed in a quartz tube inside a furnace. All the tubes are sealed gas tight with Viton O-rings.

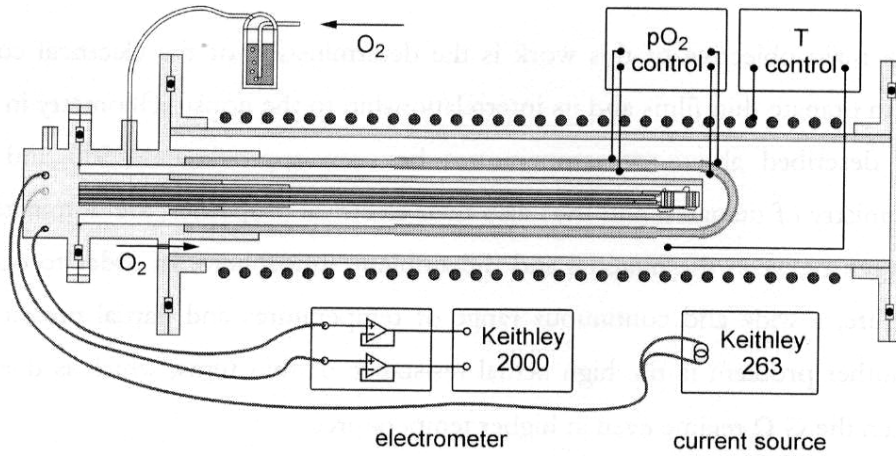
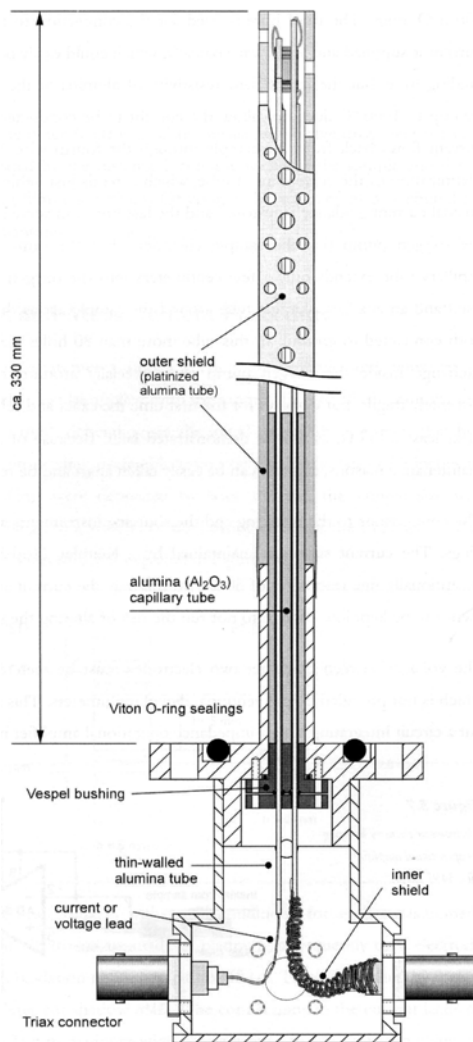


Figure 43, CT design by Ohly [7]



$V_{\text{cell}} \approx 80 \text{ cm}^3$
 $M_{\text{sample}} \approx 15 \text{ g}$
 Oxygen leakage \approx N.A.V.
 Carrier gas = H_2
 Current = N.A.V.

Figure 44, CT design by Ohly, close up [7]

Mitberg, Poepelmeier and co-workers.

Mitberg et al. [45-53] studied the electrical conductivity of several perovskite type materials (zinc doped YBCO, cobalt doped YBCO, strontium doped lanthanum cobaltate, strontium ferrite, strontium doped lanthanum ferrite, and barium doped lanthanum manganite). The samples were measured in a CT set-up, see Figure 45, to vary the oxygen partial pressure from 10^{-19} to 0.21 atm in a temperature range of 473-1223 K. The sample (1) is fixed between two thermocouples and connected with two voltage probes. The sample is placed in a cubically stabilised zirconia tube with four electrodes, two sets of two electrodes for oxygen pump (4) and sensor (3). An advantage of this design is the minimum amount of wires needed for measuring the temperature and the electrical conductivity. An additional advantage is the possibility of measuring the Seebeck (thermopower) coefficient.

The cell is evacuated and filled with a 50% O₂ and 50% CO₂ gas mixture. Low oxygen partial pressure is obtain by electrochemical oxygen pumping.

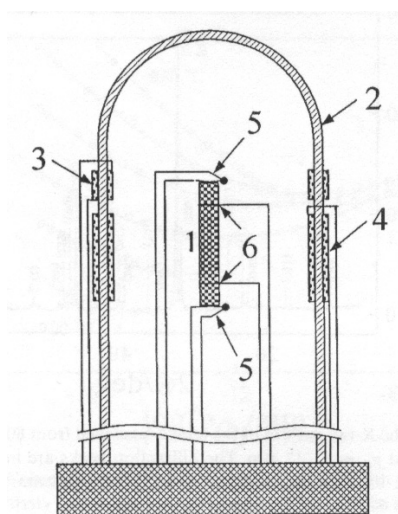


Figure 45, CT-designed by Mitberg et al. [45-51]

$$V_{\text{cell}} \approx 125 \text{ cm}^3$$

$$M_{\text{sample}} \approx 4.5 \text{ g}$$

$$\text{Oxygen leakage} \approx \text{N.A.V.}$$

$$\text{Carrier gas} = 50\% \text{ O}_2 / 50\% \text{ CO}_2$$

$$\text{Current} = \text{max } 0.5 \text{ mA}$$

Ochin et al.

The electrical conductivity of Cu_{2-δ}O in a oxygen partial pressure lower than 10^{-5} was studied by Ochin et al. [26] with the help of an electrochemical cell, see Figure 46. They obtain a lowest oxygen partial pressure limit of 10^{-7} in a temperature range of 873-1373 K. The electrical conductivity is measured by a four probe technique, four wires insulated by an alumina (16) tube are connected with the sample (15), positioned in the right part of the quartz tube (3) hold in a stainless steel tube (2). The oxygen is controlled and measured by a stabilized zirconia tube (7) covered with two electrodes (8, 9). The flanges (5) are cooled with water (4) to reduce the temperature of the furnace (1). Dried argon with 5 to 10 ppm oxygen is flushed into (13) the electrolyte tube and the amount of oxygen partial pressure is controlled electrochemically into the quartz tube (3), which is in vacuum.

$V_{\text{cell}} \approx 190 \text{ cm}^3$

$M_{\text{sample}} \approx 2 \text{ g}$

Specific oxygen leakage \approx N.A.V.

Carrier gas = argon

Current = 0.01-0.5 mA

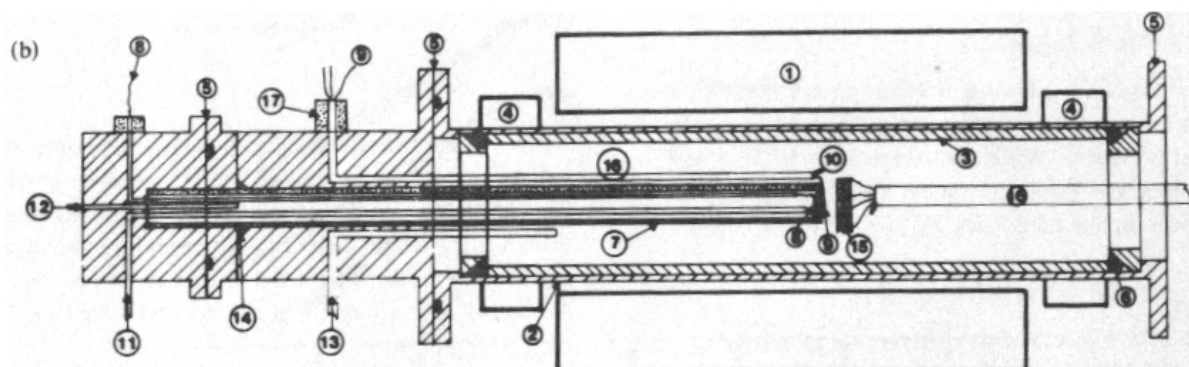
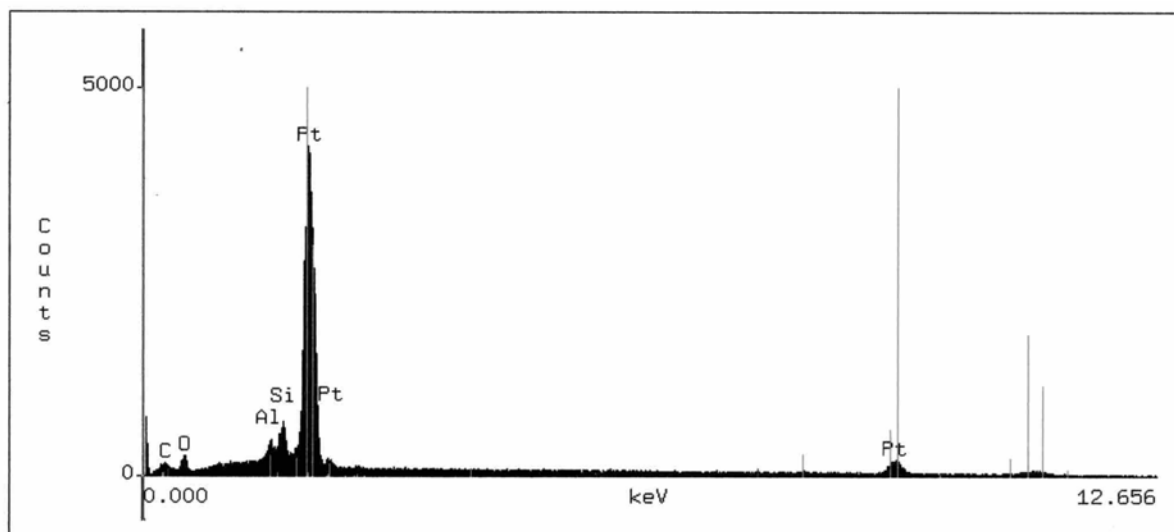


Figure 46, CT-design by Ochin et al. [26]

Appendix B – EDX results of the Platinum-Paste



Pt PASTE

Accelerating Voltage: 15 KeV

Take Off Angle: 34.4269°

Live Time: 100 seconds

Dead Time: 19.227

Wed Apr 21 12:31:29 2004

Pt PASTE

Refit "_C -K" "_C -K" "_Al-K" "_Al-K"

Refit "_Si-K"

Filter Fit Method

Chi-sqd = 17.56 Livetime = 100.0 Sec.

Standardless Analysis

Element	Relative k-ratio	Error (1-Sigma)	Net Counts	Error (1-Sigma)
O -K	0.01734	+/- 0.00112	1328 +/-	86
Si-K	0.02308	+/- 0.00059	4504 +/-	116
Pt-M	---	---	74477 +/-	544
Pt-L	0.94708	+/- 0.06046	4731 +/-	302
C -K	0.01184	+/- 0.00073	796 +/-	49
Al-K	0.00066	+/- 0.00042	132 +/-	84

PROZA Correction Acc.Volt.= 15 kV Take-off Angle=34.43 deg

Number of Iterations = 5

Element	k-ratio (calc.)	ZAF	Atom %	Element Wt %	Wt % Err. (1-Sigma)	No. of Cations
O -K	0.0152	3.233	27.18	4.90	+/- 0.32	---
Si-K	0.0202	0.989	6.31	1.99	+/- 0.05	5.568
Pt-L	0.8276	1.083	40.78	89.59	+/- 5.72	36.005
C -K	0.0103	3.334	25.50	3.45	+/- 0.21	22.517
Al-K	0.0006	1.174	0.22	0.07	+/- 0.04	0.197
Total			100.00	100.00		64.287

The number of cation results are based upon 24 Oxygen atoms

Appendix C – Micro coulometric titration cell

A coulometric titration set-up with a much smaller reactor volume (in the order of the sample volume) is required to study the conductivity, non-stoichiometry and oxygen diffusion coefficients. A possible micro coulometric titration set-up is explained in this appendix.

A quartz flushable tube is placed inside a tubular furnace, see Figure 47. The partial oxygen pressure can be varied inside the tube by mixing gases. An electrolyte bucket (bird cage) with sample is positioned inside this tube, see Figure 48.

Description:

- The quartz tube is in reducing atmosphere. The oxygen leakage is mainly determined by the reference oxygen partial pressure. Therefore, the oxygen leakage will be less.
- An electrolyte bucket painted with two electrodes on both sides. The four electrodes are used for the electrochemical cells of oxygen- pump and sensor.
- The bucket is covered with an alumina plug. A golden O-ring seals the plug and the bucket gastight.
- The sample holder is a quartz disc (slightly bended) with a horizontal coin slit. The edges of the slit and the edges of the disc are covered with Pt paste and function as two electrodes for 4-probe ‘Van der Pauw’ technique. The sample can be positioned vertically in the quartz slit and connects the electrodes with pressure due to gravity. The other two electrodes are made on a quartz bended ring or in a similar quartz slit. The weight of the ring cares for the constant pressure of the electrodes on the sample.
- The four electrodes, the thermocouple and the two negative electrodes of the pump and sensor are connected with platinum wires. The wires are transported through the alumina top and sealed with ceramic glue.

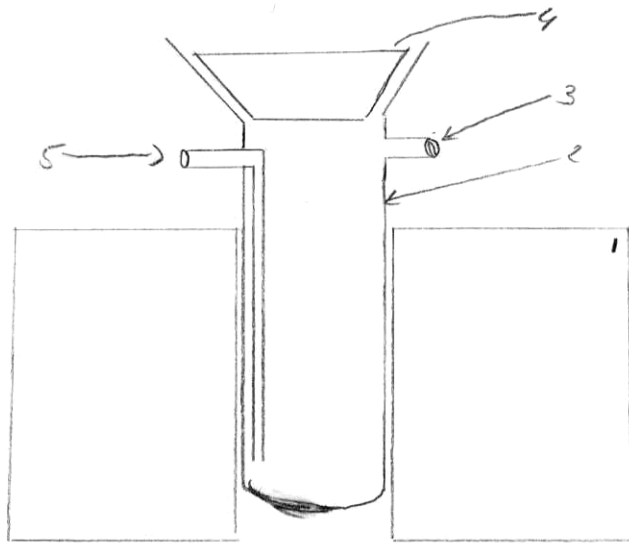


Figure 47, Micro coulometric titration set-up, overview. A quartz tube (2) is placed in a tubular furnace (1). The quartz tube with gas inlet (5) and outlet (3) tube is sealed gastight with a plug (4)

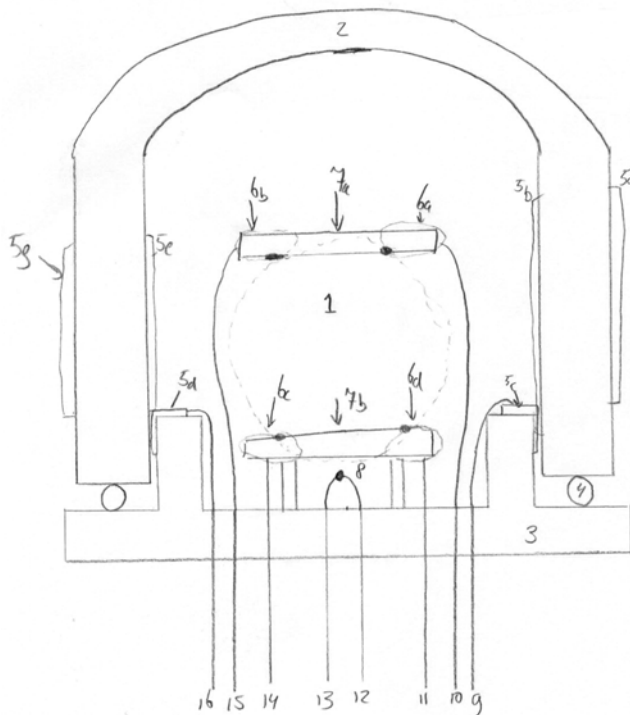


Figure 48, Micro coulometric titration set-up. The sample (1) is placed in an YSZ (2) bird cage with an alumina plug (3) sealed with a golden ring (4). The sample is fixed with two quartz discs with a coin slit (7). The temperature is measured with a thermocouple (8, 12, 13). The oxygen sensor and pump are connected with platinum wires (9 and 16). The sample is connected with 4 electrodes (10, 11, 14 and 15).

Appendix D - Defect chemistry of YSZ

The defect chemistry of YSZ can be given with the following equations. The YSZ electrolyte has an anti-Frenkel disorder. The equilibrium and the constant can be given as:



$$K_{aF} = \frac{[O_i''] [V_o^{\bullet\bullet}]}{[O_o^x] [V_i]} \quad (49)$$

The equilibrium and the constant of intrinsic ionisation can be given as:



$$K_i = np \quad (51)$$

The charge neutrality of YSZ is:

$$[Y'_{Zr}] + 2[O_i''] + n \rightleftharpoons p + 2[V_o^{\bullet\bullet}] \quad (52)$$

The acceptor (Yttrium) fixes the vacancy concentration in the middle oxygen partial pressure range. The charge neutrality equation (52) becomes:

$$[Y'_{Zr}] = 2[V_o^{\bullet\bullet}] \quad (53)$$

The oxygen vacancies are stable in this oxygen partial pressure range and therefore the gas-solid equilibrium reduces to:

$$K'_g = \frac{1}{n^4 p O_2} \quad (54)$$

$$n \propto p O_2^{-1/4}$$

$$p \propto p O_2^{1/4}$$

Yttrium cannot fix the vacancy concentration anymore at extreme low oxygen partial pressures or at high temperatures; the electrical neutrality equation (48) reduces to:

$$n = 2[V_o^{\bullet\bullet}] \quad (55)$$

$$K''_g = \frac{1}{n^6 p O_2}$$

$$n \propto p O_2^{-1/6}$$